MODULAR MULTI-SCALE ASSEMBLY SYSTEM FOR MEMS PACKAGING

by

RAKESH MURTHY

Presented to the Faculty of the Graduate School of

The University of Texas at Arlington in Partial Fulfillment

of the Requirements

for the Degree of

MASTER OF SCIENCE IN MECHANICAL ENGINEERING

THE UNIVERSITY OF TEXAS AT ARLINGTON

December 2005

ACKNOWLEDGEMENTS

With this degree, I feel one step closer to my goal. I wish to begin by thanking my Mom, Dad and my Brother.

I would like to thank Dr. Raul Fernandez for his constant support and encouragement shown in the past two years. I am indebted to Dr. Dan Popa for his support and belief in my ability. I have seen tremendous improvements in my skills and confidence under his supervision. I look forward to many more years of close association with him. I would also like to thank Dr.Agonafer for his encouragement.

I cannot undermine the role played by Dr. Jeongsik Sin, Dr. Wo Ho Lee, Dr. Heather Beardsley, Manoj Mittal, Abioudin Afosoro Amit Patil and Richard Bergs for my success in the BMC project and subsequently in my thesis research.

Finally I wish to thank all my friends from UTA and in India.

November 11, 2005

ABSTRACT

MODULAR MULTI-SCALE ASSEMBLY SYSTEM

FOR MEMS PACKAGING

Publication No. _____

Rakesh Murthy, MS

The University of Texas at Arlington, 2005

Supervising Professor: Dr. Raul Fernandez

A multi-scale robotic assembly problem is approached here with focus on mechanical design for precision positioning at the microscale. The assembly system is characterized in terms of accuracy/repeatability and calibration via experiments. The MEMS packaging requirements are studied from an assembly point of view. The tolerance budget of the assembly ranges from 4 microns to 300 microns. The system components include robots, microstages, end-effectors and fixtures that accomplish the assembly tasks. Task assignment amongst this hardware has been accomplished based on precision and dexterity availability. Various end-effectors and fixtures have been designed for use with off-the-shelf hardware (robots and microstages) to develop a coarse-fine positioning system. These end-effector and fixture designs are tested for

precision performance. The robots and the vision system are calibrated to an accuracy of 11 microns or less. Inverse kinematics solutions for one of the robots have been developed in order to position parts in the global coordinate frame. Conclusions have been drawn with regard to implementation of calibration, fixturing, visual servoing or a combination of these techniques to achieve assembly within the specified tolerance budget as required by the target application. End-effector performance is improved by tuning the PID gains of the controller such that tool oscillations are minimized.

TABLE OF CONTENTS

LIST OF ILLUSTRATIONS

LIST OF TABLES

CHAPTER 1

INTRODUCTION

1.1 Motivation- Multi-Scale Assembly

The term "Multi-Scale" in robotics refers to assembly or manipulation operations performed over a combination of scales like macro-meso-micro or meso-micro-nano. The exact nature of this combination is more specific to the problem in hand. Traditionally, the automation and robotics industries have dealt with challenges encountered in working within the framework of a single scale (macro or meso). In the past decade as micro and nano technologies have emerged and grown, several approaches towards assembly and manipulation at these scales have been proposed. We have microassembly techniques such as self-assembly and microrobotics that limit the working scale to a single level and as a parallel approach which links traditional domains to the newer domains we have multi-scale assembly.

The multi-scale approach can be used to distribute the assembly tasks into sub-components that fall into different scale-levels by selecting the advantages offered at each of these scales. The macro-meso-micro assembly technique offers a distinct advantage of combining high accuracy over a large range of motion. Microoptics packaging may involve manipulating meso/micro sized parts such as optical fibers within a few microns tolerance on a MEMS die with the fibers being few feet long. This being the case we have to use a multi-scale approach to complete the task.

Many challenges are encountered while accomplishing a multi-scale assembly process. Each of the scales have their inherent physics which may be distinct from the corresponding hand-shaking scales. Volumetric forces such as gravity dominates the meso scale manipulation while in the micro scale surface forces such as stiction and electrostatic forces dominate.[1] Factors such as this have a significant influence over mechanical design. Grippers and fixtures that make up the mechanical system have to cater to variation in dominant forces. At the micro and nano scales, gripper free manipulation is often preferred as opposed to the macro and meso scales where it is inevitable to use direct contact with grippers for part handling. Also, systems used in multi-scale solutions pose dynamic issues like vibrations which have a significant effect on the corresponding smaller scales. As we scale down from the macro or meso to the micro scales, there is a marked increase in required precision levels. Thus the challenge lies in integrating the different scales and at the same time maintaining required precision. The accuracy of robots used for handling and positioning macro and meso components need be within the working range of micropositioning systems. For example, an industrial robot used for die pick and place needs to be precise enough to place the die within the field of view of a camera or within the working range of a microstage on which a mating component, like a package is placed.

Research on microassembly techniques has been ongoing since the mid 1990's. Examples are advances made in microassembly using precision positioning stages, custom built tweezers made from LIGA, and visual servoing at Sandia and UCBerkeley [2], microscope based servoing with force feedback[3-5], microassembly system with a

six-axis robot and tool changers at the Fraunhoffer Institute [6], microassembly system using SMA microgrippers at EPFL [7], desktop microfactories in Japan, Europe and US [8,9,10], modular microassembly system using for optical fiber arrays and other microoptical components at RPI [1,11,12] and modular microassembly system based on planar linear motor positioners at CMU [13]. The results presented in this thesis describe on-going research effort in multi-scale assembly at the Automation and Robotics Research Institute at UTA.

1.2 Problem Statement

A robotic assembly cell capable of macro-meso-micro level assembly needs to be developed to accomplish MEMS die packaging used in Safe & Arm application requiring shelf lives exceeding twenty five years [24].

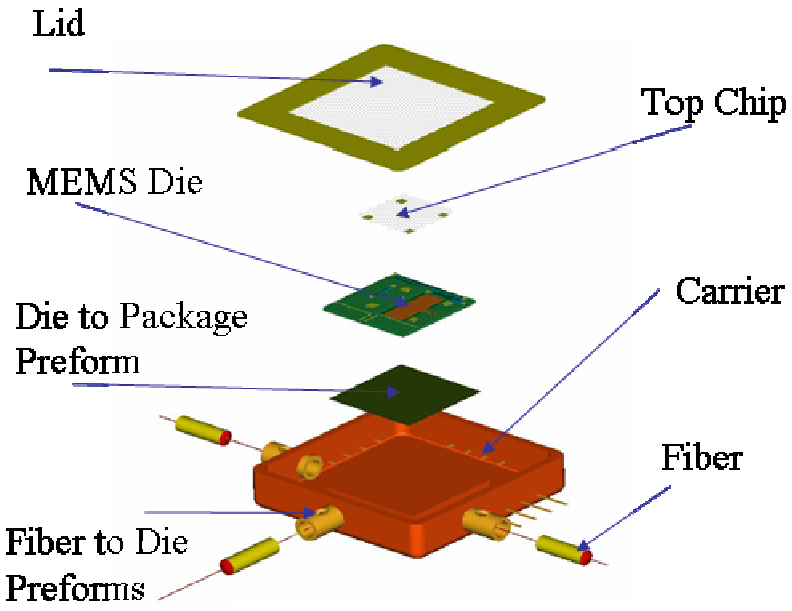

Fig 1.1 MEMS Package

End effectors and fixtures need to be designed and used with available robots to complete the assembly operation within a tolerance budget. This assembly cell requires to be capable of manipulating and positioning the package meso components with typical dimensions of about an inch or less like the MEMS die or carrier within an accuracy of a few microns. Macro components that require handling include fiber spool plates (6in X 3in X ¼ in) with grooves holding optic fibers and an enclosure (2in X 2in X 0.5in) to facilitate reducing gas environment during solder reflow.

Typical manipulation operations include

- Pick and place of package, die and performs from parts tray to the hotplate to constitute what was called "die attach".
- Optic fiber handling and insertion into package.
- Solder preform handling and laser positioning for soldering.

The objective of this research is to develop a multi-scale assembly platform that is modular and reconfigurable. We must be able to readily reuse the assembly system for a different application by changing end-effectors and fixtures.

.

1.3 Approach

For the problem statement stated above the following approach is outlined. This forms the framework of this thesis research.

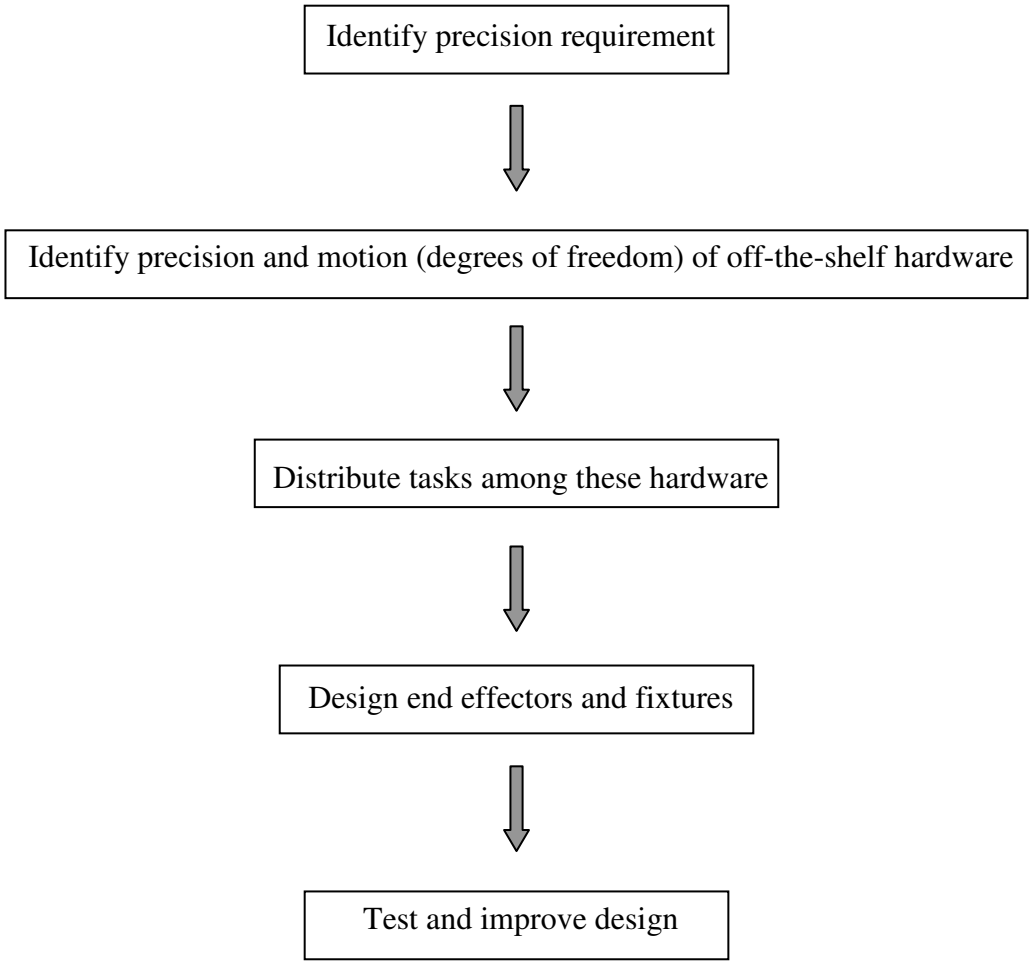

Figure1.2 Approach

We begin by investigating the tolerance set offered by the assembly. The tolerance required during positioning of every single component is studied. This is compared to the precision and dexterity offered by off-the-shelf hardware (robots) and the various assembly operations are delegated to these robots. Next, we design and fabricate end-effectors and fixtures capable of handing the parts and test their performance against assembly techniques such as calibration, fixturing and visual servoing.

1.4 Accomplishments

System Architecture: Motoman RobotWorld ® assembly platform is chosen as the basis for developing the microassembly cell. It is a modular automation work cell shared by multiple robots or pucks. The robots available for this work are a 4 axis open loop puck (x,y,z and θ), a closed loop 3 axis puck(x,y,and z) and a 2 axis XY camera puck (later modified as a 4 axis - XYZθ robot). The custom made fine positioning system consists of x, y, z axis microstages from Thorlabs ® and a rotation stage from Aerotech®. The assembly operations are listed and compared with the available positioning resources to determine the operations to be assigned to every robot. This decision is also made keeping in mind the need to separate the work volumes of the robots in order to avoid collision.

The four-axis robot is assigned the task of pick and place of the package components. As this requires the robot to handle four different end effectors, quick change adaptors are chosen to switch this robot from one tool to another depending on the operation in hand.

End-effector/Fixture design & fabrication: Vacuum pickup tools with sufficient degrees of freedom are designed for MEMS die and perform pick and place. Pneumatic grippers are designed for package pick and place, fiber insertion and handling of macro components like fiber spool plates and reducing environment enclosure. The three-axis robot is assigned the task of laser handling. Laser is one of two methods used to reflow solder during bonding process in the package; the other

technique used is a hot-plate. Fixtures necessary to support the Optical Imaging Accessory from underneath the Z axis of the robot are designed and fabricated. A platform that supports fiber insertion into the package and the reducing gas environment enclosure has been designed and fabricated. This formed the fine-positioning system of the assembly station.

Assembly system calibration/Accuracy tests: Calibration has been conducted on the camera robot and the 4 axis puck with the vacuum pick-up tool The calibration is also verified to be accurate within 11 microns. The acuracy is critical in implementing calibration as an assembly technique. The camera is calibrated first. The die is picked up by the 4 axis puck and brought under the camera. The CCD is focused to view a specific feature on the die and that is saved as a template. Using machine vision software, when the camera is moved to different locations (in global coordinate frame), pixel readings related to the template feature are noted. Different positions of the camera robot and the corresponding pixel locations are tabulated. Using these in the kinematic equations of the camera, the transformation matrix relating the CCD to the Robot is derived. This relates the CCD coordinate frame to the RobotWorld coordinate frame. Next the robot is moved to different locations along different axis (x, y andθ). For each position, the corresponding 4-axis robot location, camera location and CCD pixel readings are noted. These, along with the CCD to Camera transformation matrix are plugged into the 4-axis robot kinematic equations and solved to derive the transformation matrix that relates the feature on the die to the global coordinate frame. Next, the calibration routine followed for the robots is verified. The 4-axis robot is

driven to a new location in the work volume. The camera is now moved to view the die. This gives us a new location for the camera, robot and the corresponding pixel readings for the template feature. Using the camera calibration equations we can now locate the die in the RobotWorld coordinate frame. Next we use the robot calibration equations and map the die to the RobotWorld coordinate frame. It is found that this location matches in close proximity (within 11 micron error in X and Y) to the location derived from the camera calibration.

Inverse kinematic equations need to be developed and used to provide a means of referencing the parts in RobotWorld coordinate frame. For example, specific features on the die that aid in alignment of die to package can be identified and then the robot can be moved to a calculated orientation (using inverse kinematic equations) to position the die inside the package.

The knowledge of the positioning accuracy and repeatability of the robots is necessary to validate the design compatibility with tolerance budget offered by the problem in hand. More-so when the 4 axis robot switches tools via the quick change mechanism and parts are vacuum picked using the vacuum pickup tool. Experiments to determine the accuracy and repeatability of the camera and four axis robots have been conducted. Based on the calibration experiments and the accuracy/repeatability experiments, certain design/assembly rules pertaining to the usage of fixturing or calibration or visual servoing or their combination are implemented.

PID gain tuning is essential to minimize oscillations caused during part handling. The end-effectors are offset from the center of the robot and these offsets

cause oscillations during robot operation. Gain tuning is performed specific to the tool-manipulator combination to minimize the effect of these oscillations.

1.5 Summary

A robotic assembly cell with multi-scale capability has been developed. Various mechanical tools and fixtures have been designed, built and tested to suit a packaging assignment. The vibrations that occur with these tools have been minimized by PID tuning followed by accuracy tests, which have been conducted to determine the exact positioning accuracy of the robots and vision system. Robot calibration has been conducted and verified to an accuracy of 11 microns. An inverse kinematic solution has been developed for the four-axis robot with die handling tool to accomplish die attach within acceptable accuracy limits.

CHAPTER 2

BACKGROUND

2.1 Microassembly

Microassembly deals with assembly of components whose dimensions lie between the conventional macro-scale (>1mm) and the molecular scale (<1μm)[16]. It involves positioning, orienting and assembling of microscale components into complex microsystems. In short, microassembly can be defined as the assembly of objects with microscale and/or mesoscale features under microscale tolerances. In the past decade significant progress has been achieved in microassembly, gripping, handling, positioning and bonding of parts with dimensions between a few microns to several millimeters [3, 11, 13, 14, 15, 16]. Due to the small size of these components, fairly specialized microgrippers, fixtures and positioning systems have been developed [17-22].

Need: Current microsystems generally use monolithic designs in which all components are fabricated in one (lengthy) sequential process [16]. In contrast to the more standardized IC manufacturing, a feature of this manufacturing technology is the wide variety of non-standard processes and materials that may be incompatible with each other. These incompatibilities severely limit the manufacture of complex devices. The goal of microassembly is to provide a means to achieve hybrid micro-scale devices of high complexity. Manufacturing hybrid microsystems poses many unique challenges to

fabrication, packaging and interconnection techniques. As an enabling technique, assembly plays an essential role in addressing these challenges. The functions of assembly in microsystems manufacturing are similar to those in conventional macroscale manufacturing. However, in terms of manipulation, assembly in microsystems manufacturing is significantly different from that in both microscale manufacturing and IC manufacturing.

Challenges: Assembly of micro components is associated with high precision requirements. There is a demand to work at a few micron part sizes or at a few micron tolerance.

Mechanically, it is difficult to use grippers because of the interaction forces between grippers and parts. Also, the absolute position of parts and tools are much more difficult to measure for microassembly.

Scaling effects also pose a challenge. Most microassembly solutions employ conventional assembly concepts scaled down to the microscale, though their effectiveness diminishes as part dimensions shrink below 100μm [1]. For parts with masses of several grams, the gravitational force will usually dominate adhesive forces, and parts will drop when the gripper opens. For parts with size less than a millimeter, the gravitational and inertial forces may become insignificant compared to adhesive forces, which are generally proportional to surface area. When parts become very small, adhesive forces can prevent release of part from the gripper.

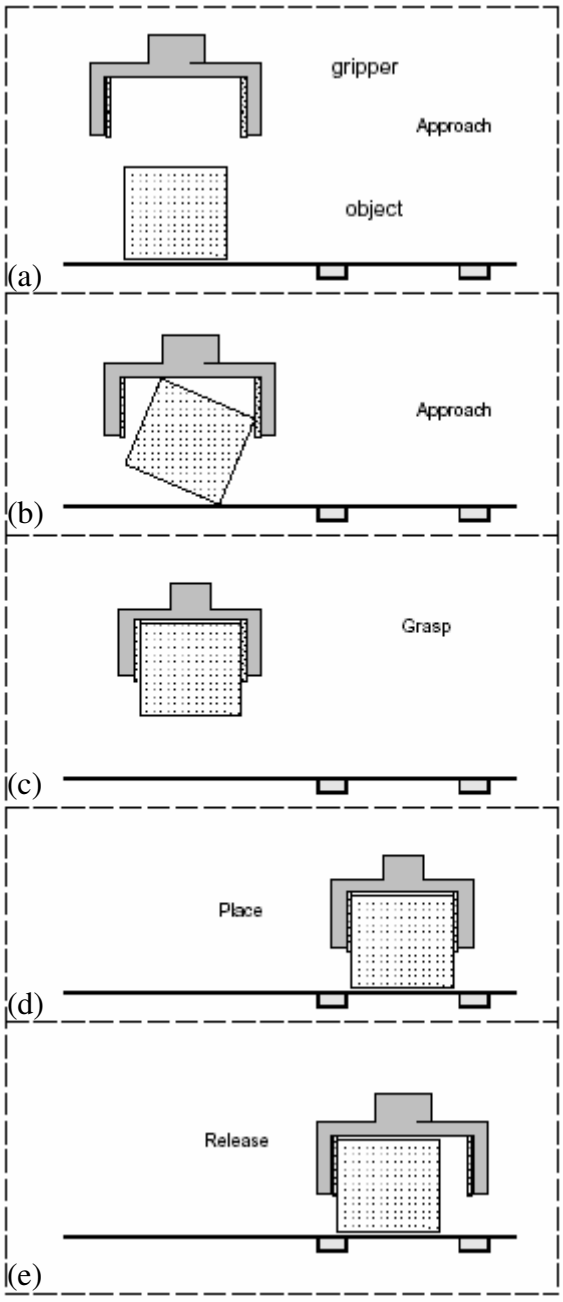

Fig 2.1 “sticking effect” in microassembly; (a), (b) approach, (c)Grasp, (d) Place, (e) Release

Classification: The techniques currently in use for microassembly are serial microassembly and parallel Microassembly [16].

In serial microassembly, parts are put together one-by-one according to the traditional pick and place paradigm. Serial microassembly may include manual assembly with tweezers and microscopes, visually based and teleopertaed microassembly, use of high precision macroscopic robots and microgrippers.

Parallel microassembly involves multiple parts (identical or different design) being assembled simultaneously. This can be either deterministic or stochastic. In the deterministic category the relationship between part and its destination is known, while in the stochastic category this relationship is random or unknown. The parts involved in stochastic microassembly "self-assemble". Some examples of the motive forces that cause this self-assembly can be fluidic agitation and vibratory agitation.

2.2 Precision assembly

Passive, active or a combination of the two styles of compliance can be incorporated into an assembly station to maintain a high level of precision. RCC (Remote Center Compliance) is a passive compensation device. Misalignment during assembly or operation can consist of lateral and angular errors. The errors can be due to machine inaccuracy, fixturing tolerances or part vibrations. One was to compensate for these positioning errors is to include compliance laterally and angularly, so as to allow an assembly machine or robot to compensate for positioning error.

Principles of RCC: There are four basic stages for a part mating (assembly of a peg into a hole). 1. Approach-this occurs when the robot brings the peg into the hole. 2. Chamfer crossing- this happens when the robot initially starts to insert the peg. 3. One point contact-the peg and the hole make side to side contact along their cylindrical side

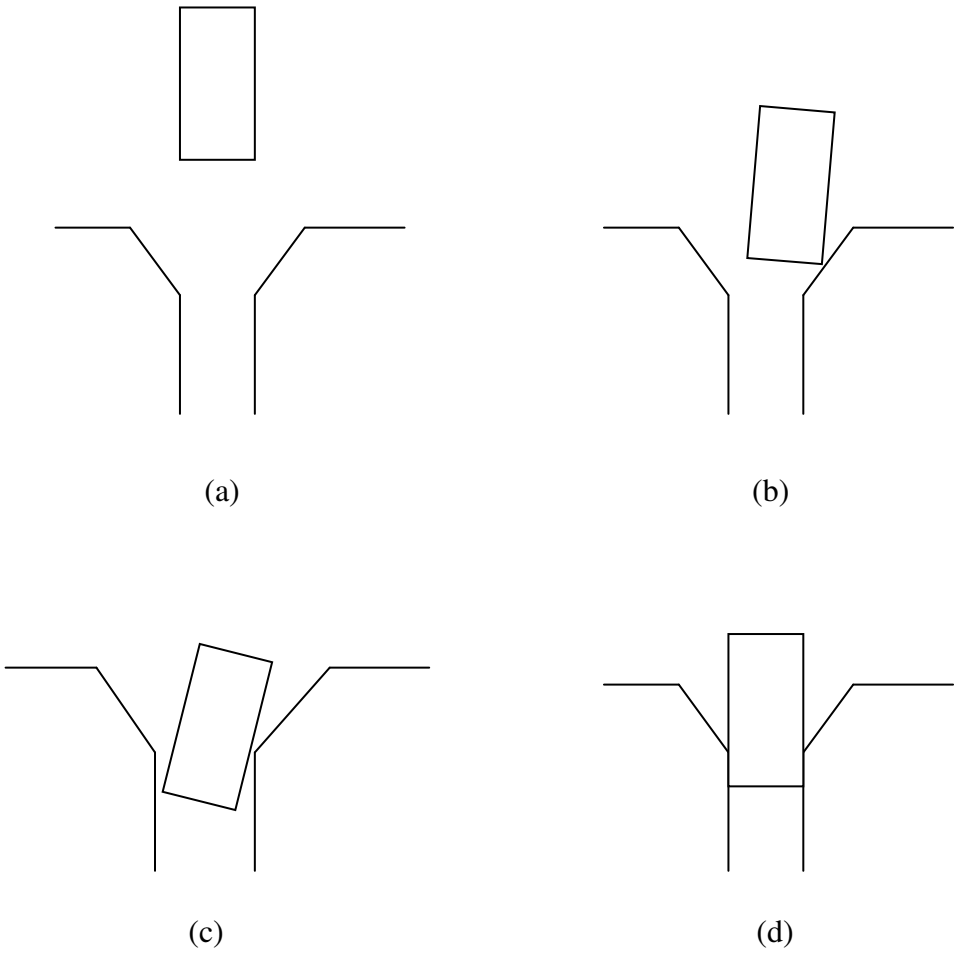

Fig 2.2 Principles of RCC, (a) approach, (b) chamfer crossing, (c) one point contact, (d) two point contact

surfaces at one and only one point. 4. Two Point contact-the cylindrical surfaces of the hole and the peg make contact at two points that join with a line drawn through the longitudinal axis of the peg. The second type is the active method which uses a controllable device to adjust actively during the parts mating process.

2.3 Errors in Manipulators

Physical errors in manipulators can come from many sources. Some of them are listed as follows [24]:

- *Machining Errors*: These errors are resulting from machining tolerances of the individual mechanical components that are assembled to build the robot
- *Assembly*: These errors include linear and angular errors that are produced during assembly of various components that are assembled to build the robot.
- *Deflections*: Errors can occur due to deflection of joints and links.
- *Measurement and Control*: Measurement, actuator and control errors will create end effector positioning errors. The resolution of encoders and stepper motors are example of such errors.
- *Clearances*: Backlash errors can occur in the motor gear box and in the manipulator joints.

Errors are also repeatable and random [25]. Repeatable errors are errors whose numerical value and sign are constant for each manipulator configuration. An example of a repeatable error is an assembly error. Random errors are errors whose numerical value and sign change unpredictably. An example of a random error is the error that occurs due to backlash of an actuator gear train.

2.4 Modular/ Reconfigurable assembly system

Microfactory: The microfactory as defined by the University of Tokyo, is a means of achieving higher throughput with less space and reduced consumption of both resources and energy via downsizing of production processes. Costs of microsystems is dominated by production costs. Microfactories have the potential for reducing production costs due to lower investment and less energy required. They carry the advantage of producing at high speed due to lesser masses to be moved and shorter distances to be traveled. They are also modular and can be modified easily to suit changes in production type.

Minifactory: The SCARA (Selective Compliance Assembly Robot Arm) manipulator is a popular choice for most automated assembly systems. However, typical SCARA's used in assembly have motion resolution and repeatabilities of 50 to 100 μm at best [13] which severly limits their use in high precision work. As a counter-measure, an alternative robot configuration has been developed which provides the same four degrees of freedom as a SCARA but which greatly ameliorates this problem.

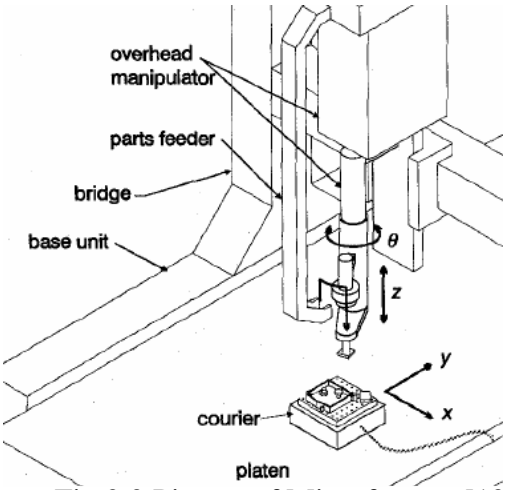

Fig 2.3 Picture of Microfactory [13]

The θ_3 axis and the z axis of the SCARA are retained fixed in work-space. The θ_1 and θ_2 axes are discarded in favor of a X, Y stage robot called the "courier". This robot carries the subassembly. Moreover, this robot is implemented as a two axes linear motor capable of traveling above a flat platen surface over a large workspace. An important feature of this setup is that each of the 2 DOF robots can be an order of magnitude smaller in size than a typical SCARA for assembling the same size product. This leads to a large increase in achievable precision. The modularity of this system lies in the fact that segments of a microfactory can be modified or extended with minimal or no impact to the neighboring or any other part of the mini-factory.

2.5 Visual Servoing

Visual servoing is one of the approaches to the control of robot manipulators that is based on visual perception of robot and workpiece location. More concretely, visual servoing involves the use of one or more cameras and a computer vision system to control the position of the robot's end-effector relative to the workpiece as required by the task. It is a multi-disciplinary research area spanning computer vision, robotics, kinematics, dynamics, control and real-time systems [26].

Visual servoing is an alternative to precise calibration. Traditionally, the feedback provided to the assembly process by vision sensors has been incorporated into the assembly process outside of the manipulator control loop. In visual servoing, we place the vision sensor within the feedback loop of the manipulator. Using visual feedback effectively in the control loop of an assembly process presents challenges

quite different from those presented by othe feedback techniques like force feedback. The large amount of data collected by a visual sensor causes the sampling rate to be relatively small, and introduces large delays in the control loop. Since noise exists in visual sensors and the sampling rate is low, robust feature trackers and control algorithms must be used.

CHAPTER 3

SYSTEM ARCHITECTURE

3.1 Parts to be assembled

The package in its assembled form is shown in the figure 3.1. The package component's sizes span over the meso and micro scales. Figure 3.2 shows an exploded view of the package.

A Kovar ® carrier houses the entire package. The carrier is about 1'' x 1'' in size and 0.25 inches in height. Kovar is an Iron based alloy with Cobalt and Nickel.

The MEMS die is a Deep Reactive Ion Etching (DRIE) Silicon On Insulator (SOI) chip. The die is 12mm by 12mm in area. Fabricated on it are optical switches and trenches in which optical fibers are inserted. The four trenches are 130 microns wide and deep. The optical fibers are inserted through the carrier onto the die.

The optical fibers are 126 microns in diameter with Au coating at the tip. These fibers are 2 feet long.

The preform that solders the die to the carrier is a Au-Sn eutectic alloy. It has a thickness of 25 microns. This preform reflow is performed using a hot-plate.

The glass top chip sits on the MEMS die and is soldered onto it using Indium solder pads deposited on the die. This has an area of 7.5 mm by 7.5 mm. The functionality is to protect the MEMS die and to prevent the fiber from coming off the die trench.

Indium preforms solder the fiber onto the carrier. These preforms are cylindrical in shape and have a diameter of 2mm and height of 4.5 mm. They are dropped into holes in the carrier and soldered using laser in a reducing gas environment to prevent their oxidation.

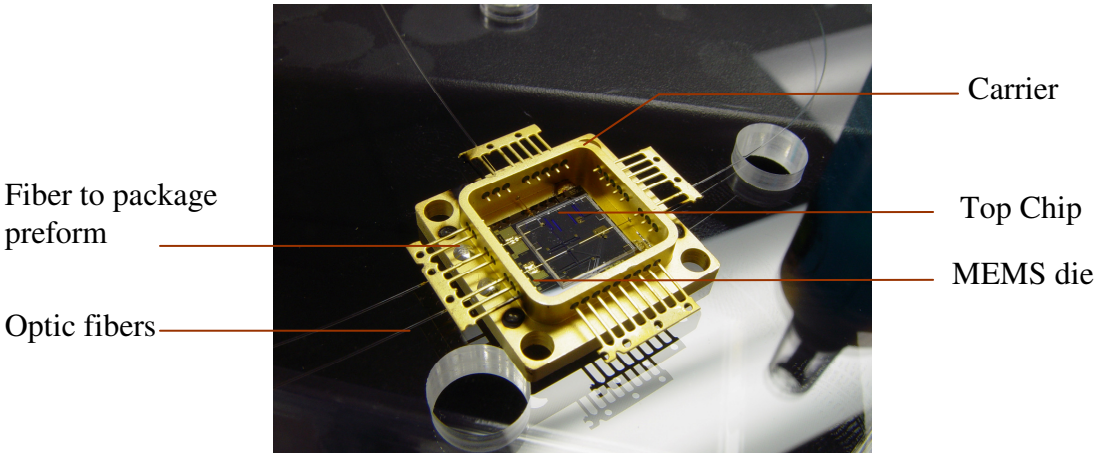

Fig 3.1 Completed package

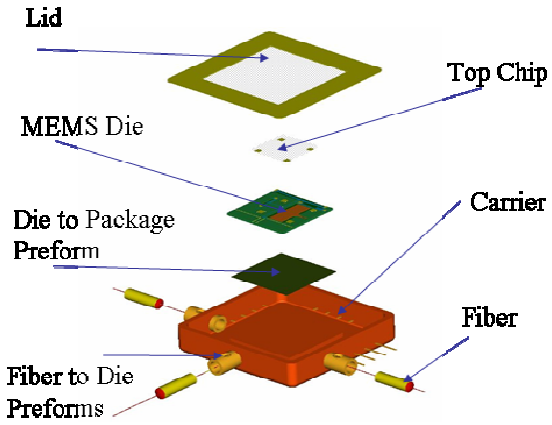

Fig 3.2 Exploded view of components to be assembled [24]

3.2 Assembly Sequence

The multi-scale assembly sequence followed to assemble the package components is described here. Different components require different criteria for assembly. Depending on the component type and the processes involved in attaching it to the package body, specific robot end-effectors and fixtures need to be designed. The overall packaging operation can be divided into two subsets of operations:

Die Attach: This is the sequence of operations followed to attach the MEMS die and the top chip into the Kovar carrier. The stacking up of the components into the carrier is performed on a hot plate. The following are the operations/manipulations involved.

a. The Kovar carrier is picked from the parts tray and placed on the hotplate.
b. The 80Sn-20Au eutectic die preform is picked from the parts tray and placed inside the package.
c. The MEMS die is picked from the parts tray, aligned to the carrier and placed on the preform.
d. The top-chip is picked and placed on the die such that the preform pads on the die are aligned to the matching pads on the top-chip.

This constitutes the "stack" of components inside the carrier. Following this is the process of re-flow of the preform by turning on the hot-plate to a temperature of $350^{O}C$.

Fiber Insertion and Attach: This involves optical fiber insertion into the package followed by preform re-flow.

a. Following die-attach, the package is picked from the plate and placed on the fiberspool plate (see section) which constitutes the fine manipulation system along with the microstages.
b. Optical fiber is inserted into the carrier, indium preform is dropped into the carrier on the hole corresponding to the fiber.
c. A 60W Coherent® Quattro-FAP semiconductor diode laser is used to melt indium that attaches the fiber onto the package. Operations 'a' , and 'b' are repeated for the other three fibers.

In addition to these, we have other manipulations related to fiber handling like staging the fiber around the carrier before it can be inserted and providing a reducing gas environment. All of these operations are described in greater detail in the subsequent sections.

3.3 Precision Requirements

This section describes the tolerances permitted in positioning the components of the package. Termed "Tolerance Budget", these set of numbers constitute the basis for the design and operation of the system. The gold coated optic fiber is 126 microns in diameter and is inserted through the sidewall of the Kovar® package into a Deep Reactive Ion Etching (DRIE) trench on the MEMS die. The fiber is constrained by the trench in X,Y and by the die+ top chip in Z. The pitch and yaw are constrained by the

feed through geometry in the package sidewall which has a tapering hole to feed the fiber through it. The larger opening is 762 microns in diameter and the smaller opening is 508 microns. The DRIE trench is 130 microns in width and is 130 microns deep. The fiber is held in the trench by the top chip (not shown in figure 3.3)

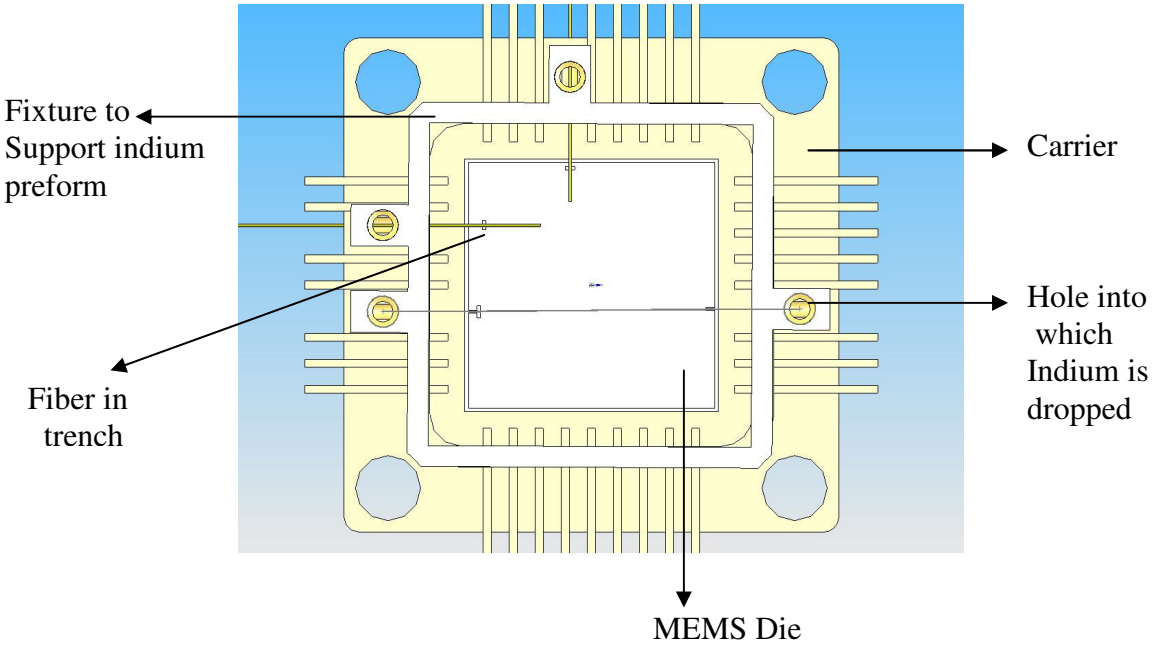

Fig 3.3 Package alignment

The tolerance budget outlined in table 1 can be explained with reference to figure 3.4.

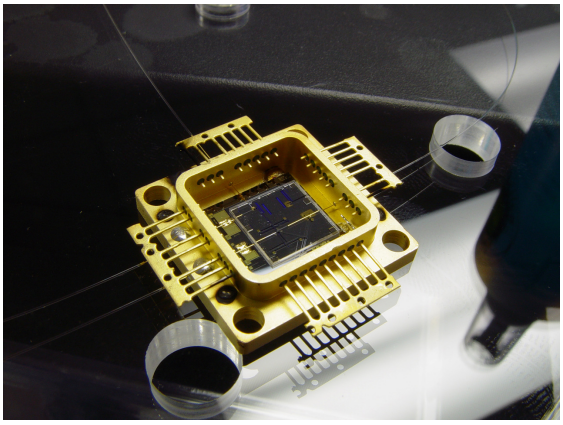

(a)

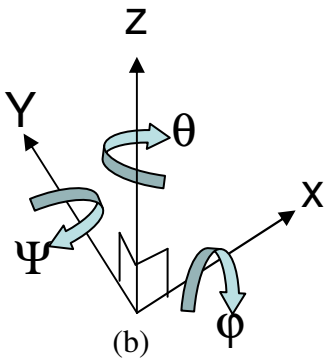

(b)

Fig 3.4 Tolerance budget description;(a) package, (b) coordinate frame

The die to package tolerance is the tolerance offered when all the four fiber trenches in the MEMS die are aligned to the corresponding four holes in the carrier. The fiber to package tolerance is the tolerance permitted in inserting the optical fiber into the outer hole on the Kovar carrier sidewall. The carrier has four tapering holes on its sidewalls for inserting the fiber through them. The outer hole has a 762 micron diameter. Fiber to trench tolerance is the clearance between the trench on the MEMS die and the optical fiber. The optical fiber in constrained by the die on three sides and the glass top chip on the top. The glass top chip has square pads which have to match with the corresponding solder pads in the die. The tolerance offered in doing this is referred to as the top chip to die tolerance in table 1. The Indium preforms are cylindrical in shape. These preforms are dropped into the carrier that has four circular openings perpendicular to the holes into which the fibers are inserted

. Table 3.1 Tolerance budget

tolerance in microns and degrees	ΔX	ΔY	ΔZ	Δθ (Yaw)	Δφ (Pitch)	Δψ (Roll)
Die to Package	50	50	25	0.5	---	---
Fiber to Package	300	300	186	0.859	0.859	---
Fiber to Trench	04	04	25	0.2	---	---
Top Chip to Die	50	50	25	0.22	---	---
In Preform to Package	127	127	---	---	8	8

3.4 System Components

The multi-scale assembly system comprises of many sub components which aid coarse-fine motion and machine vision.. The multi-scale assembly cell comprises of an automation workcell called RobotWorld® shown in figure 3.5.

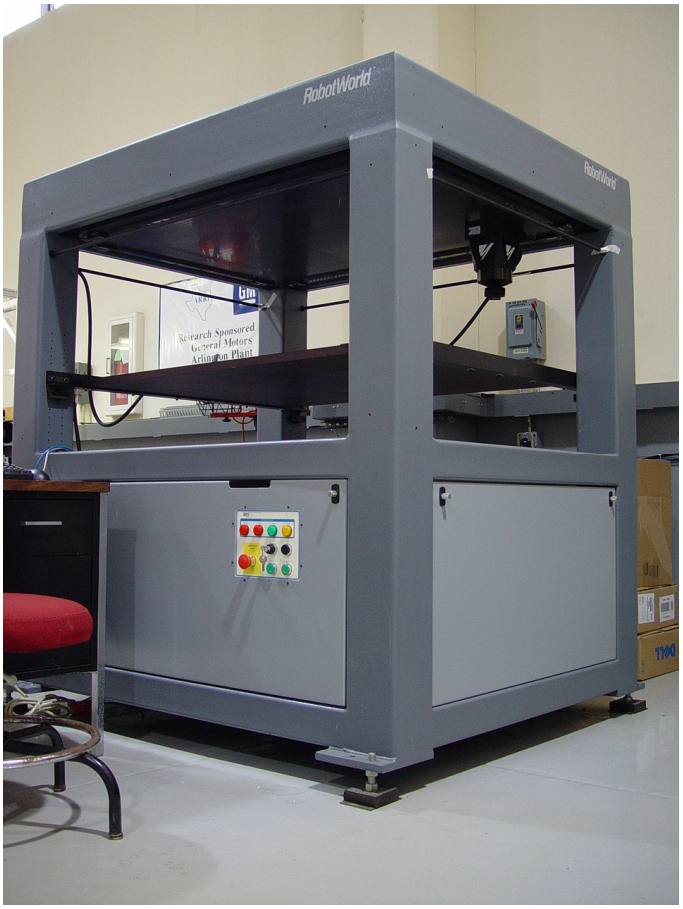

Fig 3.5 RobotWorld® setup

The components are described here in detail

a) Coarse Positioning System: The workcell consists of multiple robots. These robots are Cartesian with degrees of freedom ranging from 2 to 4.

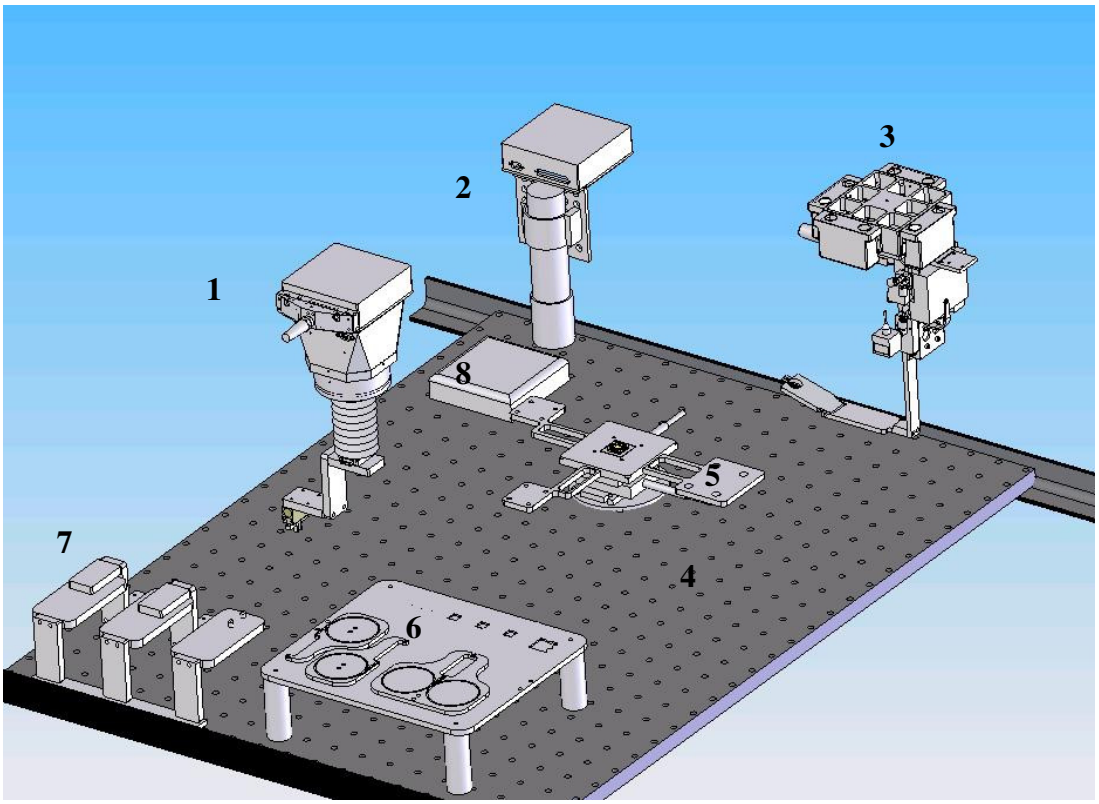

Fig 3.6 Multi-scale mechanical setup

1. Four axis (XYZθ) coarse manipulator robot
2. Four axis (XYZθ) coarse camera robot
3. Three axis (XYZ) fine manipulator robot
4. Optic Bread-Board
5. Three Axis (θXY) microstages (robot)
6. Parts Tray
7. Tool Rest
8. Hot Plate

From figure 3.13, system (1) is A 4DOF (XYZθ) manipulator consisting of a RM6210 RobotWorld® puck, which includes integrated I/O and pneumatic. (2) is a 4DOF (XYZθ) mobile camera module consisting of a 2DOF CM6200 RobotWorld® puck base that carries a VZM 450 motorized zoom microscope, and a Thor Labs PT2-Z6 stage (for autofocus). (3) is a 3DOF (XYZ) manipulator based on a RobotWorld® TM6200GT closed-loop puck. (5) is a 3 DOF (θXY) manipulator based on an Aerotech ART 315 rotational stage carrying two Thor Labs PT2-Z6 stages. Shown in figure 3.14, this manipulator is a fine positioner, and is used as the holder platform for the package during the fiber insertion and attachment processes.

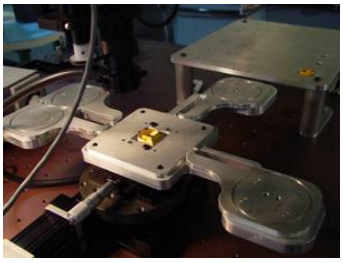

(a)

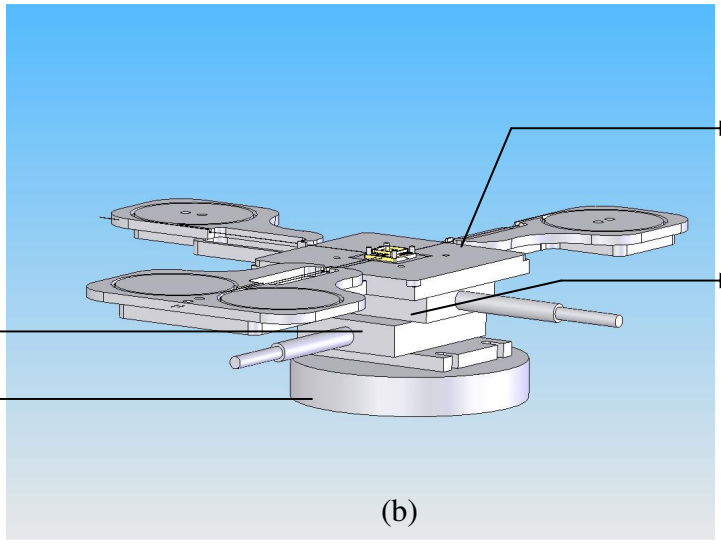

(b)

Fig 3.7 Fine positioning system,(a) platform, (b)solid model

The four axis robot (1) is configured to operate multiple tools with a Advanced Robotics ® XC-1 quick change adaptor. Thus this robot operates the carrier gripper, vacuum pickup tool, fiber gripper and the indium solder pickup tool. The three axis robot (3) used for laser positioning with motion along X, Y and Z.

We use a custom supervisory controller implemented in Labview ™ running on a Windows PC to integrate the assembly sequences, as shown in Figure 3.15. The PC communicates via TCP-IP with the host RobotWorld® controller through ActiveX commands. The supervisor communicates with the zoom camera via a National Instruments IMAQ card and vision library, and with the microstages using the NI-PCI7358 8-output motion control board and the NI Motion library.

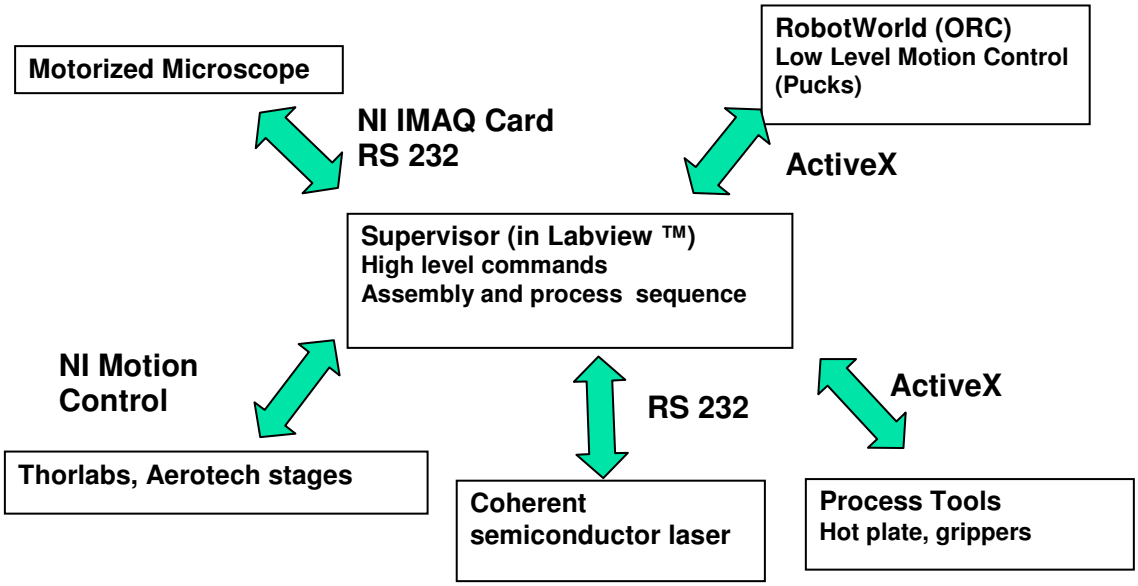

Fig 3.8 Schematic diagram of supervisory control system

3.5 End-Effector/Fixture Design

Various end effectors have been designed to be used in conjunction with the robots. These end effectors have been designed to suit specific manipulation requirements enlisted in section 3.2.

Generic Offset(s) Calculation: The RobotWorld ® pucks or robots occupy the available working volume in an inverted Z fashion, upside down from the top (platen) to the optic platform at the bottom. While systems like microstages, hotplate etc and fixtures like parts tray, tool rests, etc are placed on the optic breadboard the robots reach from the top to access them. We have designed tools incorporating this compensation in Z. Also, when two pucks are coordinating an operation at the same time, we will have them offset from the exact location of manipulation. For example when the camera robot is viewing a die placement operation, the camera is right above the die. The tools which carries the die is on the second robot which will have to operate from a distance in order to avoid collision with the camera robot. Thus we need to design X, Y and Z offsets in the tools. The exact value of these offsets is tool and operation specific.

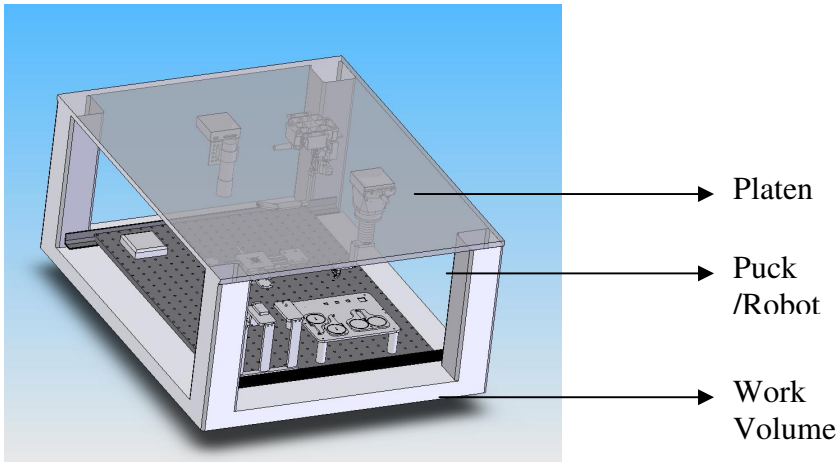

Fig 3.9 RobotWorld setup shown with platen (translucent)

The end effectors are described in the following section.

A. Carrier Gripper:

Functionality: This end-effector has been designed to handle the carrier. The carrier has on four corners (shown below) holes that may be used for positioning and manipulation.

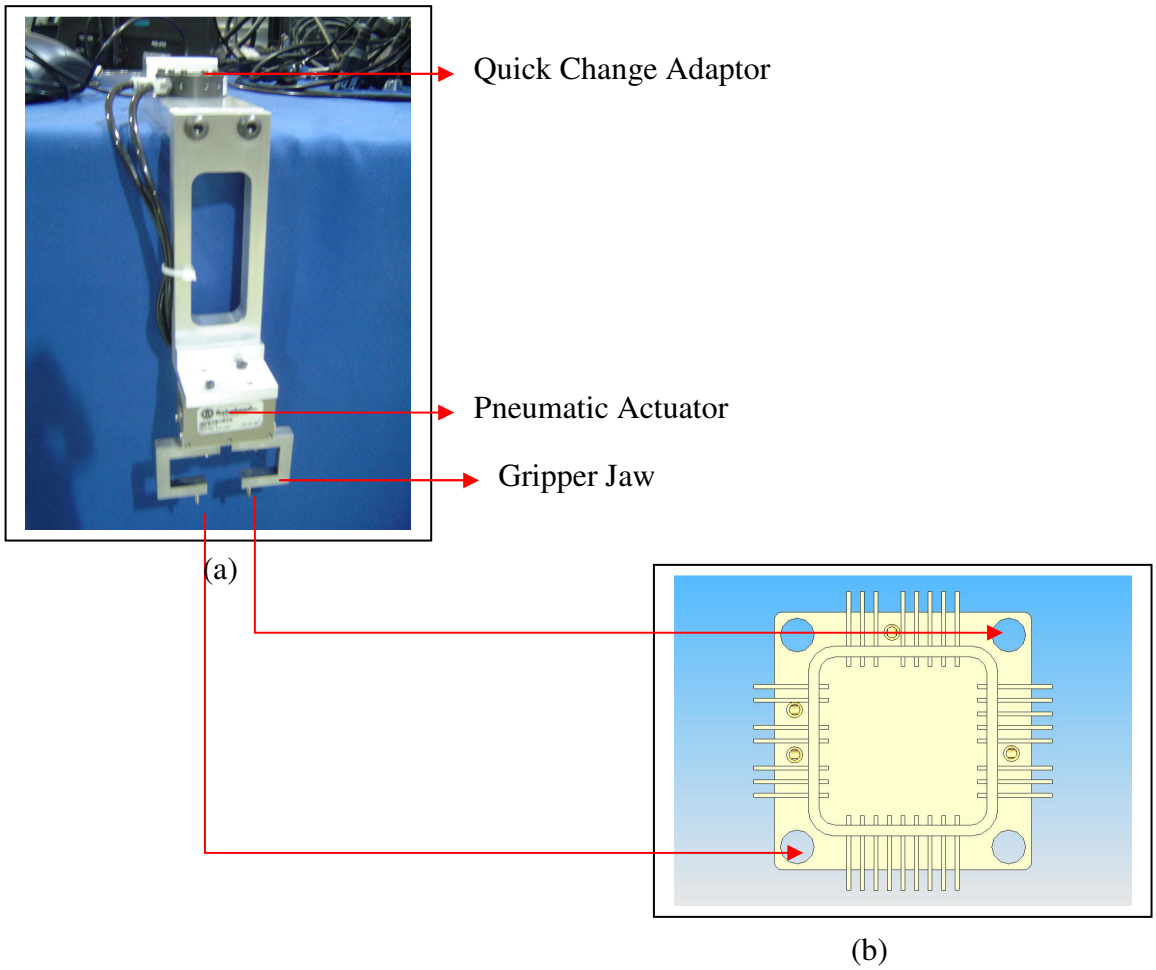

Figure 3.10 Package gripper (a) gripper, (b) carrier

Operation: The gripper has two jaws that open and close pneumatically at an operating pressure of 65 psi using RoboHand® RPLC-1 actuator. In their open position, the two jaws slide into the diagonally opposing holes of the carrier (shown in figure 3.9).

Other applications: This end-effector is also used to handle fiber-spool plates as well as the enclosure used to produce reducing gas environment. This serves as a multi-purpose end –effector. The four axis robot operates this tool via the Advanced Robotics XC-1 ® quick change adaptor (shown in the figure 3.5).

B. Vacuum Pick-Up Tool

Functionality: This tool is used for pick & place operations of the MEMS die, the die to carrier perform and the top chip.

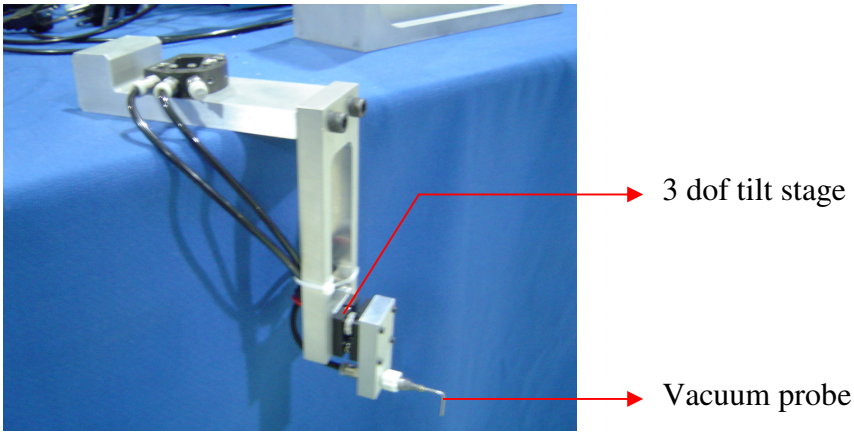

Figure 3.11 Vacuum pick-up tool

Operation: The vacuum line runs through the quick change and connects to the probe. It has the XC-1 ® quick change adaptor that facilitates usage with the four axis robot. A three degree of freedom tilt stage as shown permits setting the orientation of the tip such that the dies picked up are perfectly horizontal. This is critical to facilitate accurate pick up and placing of the components.

C. Fiber Gripper

Functionality: This tool is designed to grip the optic fiber while fiber insertion is carried out on the microstages.

Operation: The fiber gripper consists of two opposing jaws that pneumatically open and close. The fiber is pushed against a grove on one of the jaws by the second jaw.

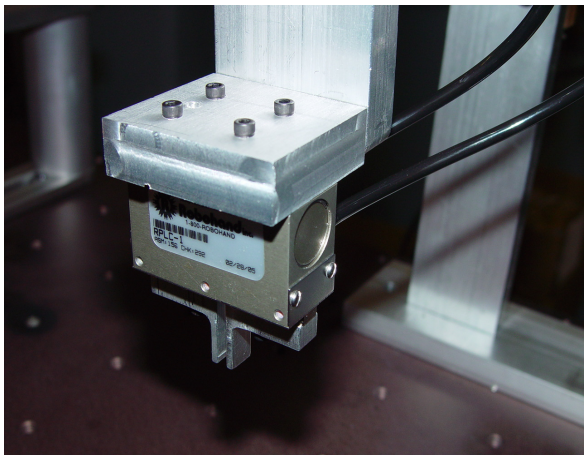

Fig 3.12 Fiber gripper

D. Indium Pick-Up Tool:

Functionality: This vacuum operated tool is designed to pickup and drop cylindrical indium performs from the parts tray into the carrier for fiber attach.

Operation: Much like the “Vacuum Pick-up Tool”, this end effector has a vacuum probe with a tilt stage. It also has a quick change adaptor and is operated with the four axis puck.

E. Tool Rests: The tools described in the above sections are rested on the fixtures shown while not in use by the robot (shown in figure). Each tool has the exact same set of clearance holes that slide into the steel pins on the mating fixture plate. Currently in the present setup we have four such fixtures in use for the four tools. The four axis robot has the male quick change adaptor that mates with the female side of the quick change adaptors on each of the tools.

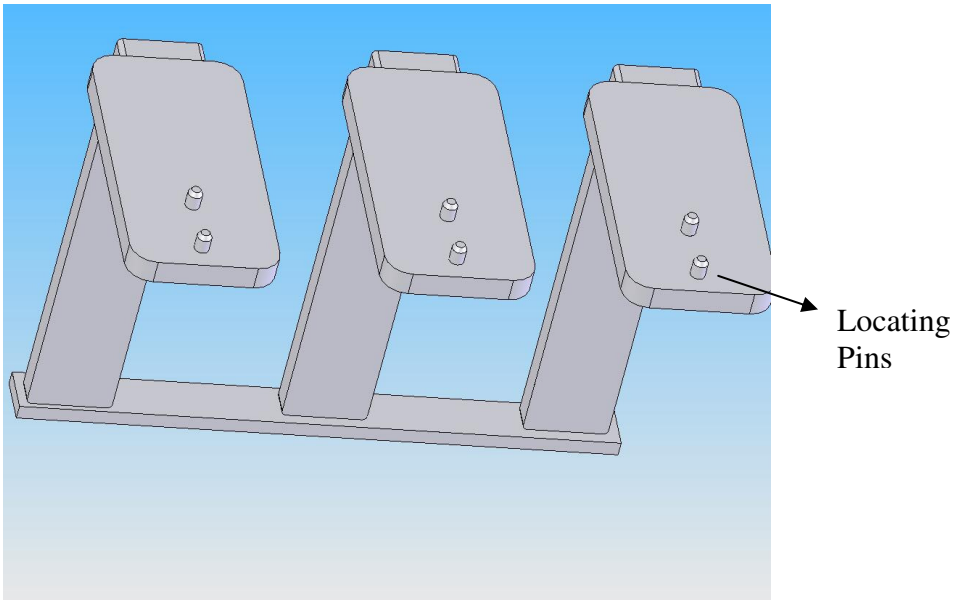

Fig 3.13 Tool rest fixtures

A note on modularity: All the end effectors described here have similar quick change adaptors attached in the same orientation and locations on the tools. The plates designed for the end effectors are very similar to each other and are interchangeable from tool to tool. The clearance holes on these tools which enable them to be placed on the tool rest fixtures are located in the exact same locations on all tools. This adds to the mechanical

modularity of the system. Any new tool designed requires minimal mechanical changes in the tool design and no change in the fixtures used for tool resting.

F. Fiber insertion platform:

The fiber insertion and soldering operations are carried out by placing the package on a set of microstages capable of high resolution linear and rotary motion. The fiber insertion platform (shown in the figure) is a multi purpose design which serves the following purposes:

a. Facilitates fiber insertion by locating carrier with respect to fiber spools on three sides of the carrier.
b. Supports reducing gas enclosure while indium preforms reflow occurs.
c. Facilitates purging of reducing gas enclosure by supplying (N_2 + H_2) gases internally.
d. Thermally isolates the microstages from the heat produced during laser soldering of indium preforms.

Fiber handling with this platform: In the figure 3.9, the transparent parts are metal plates that carry spools of fiber which are two feet long. They are wound on the circular groove and presented at one end of the plate, where a rectangular slot is cut out to accommodate the fiber gripper.

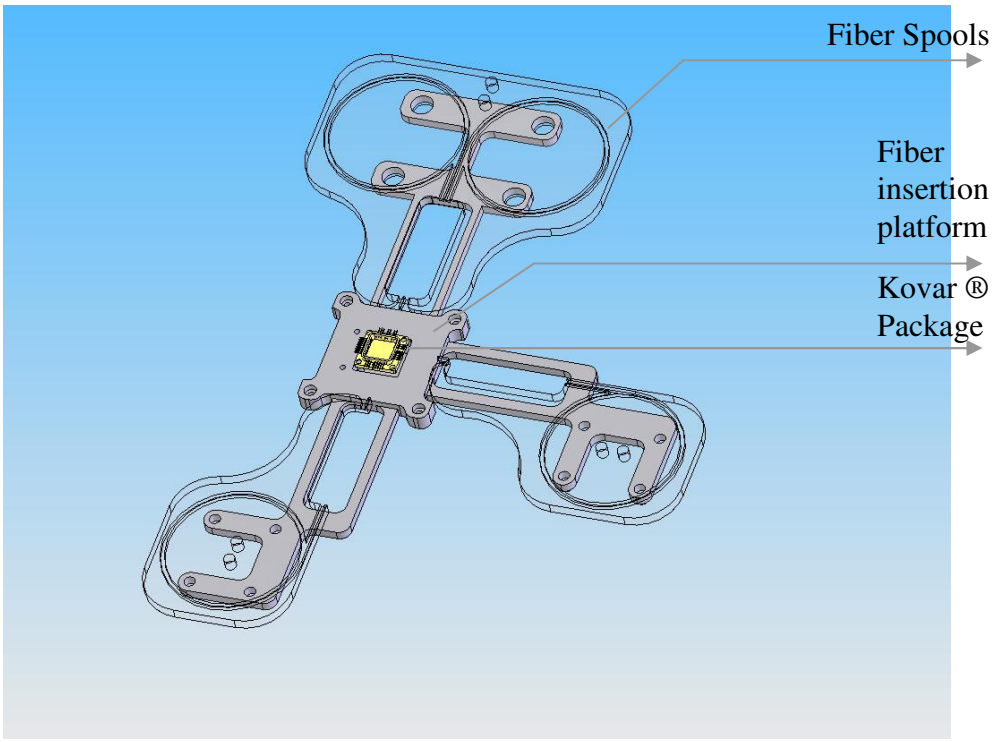

Fig 3.14 Fiber insertion platform

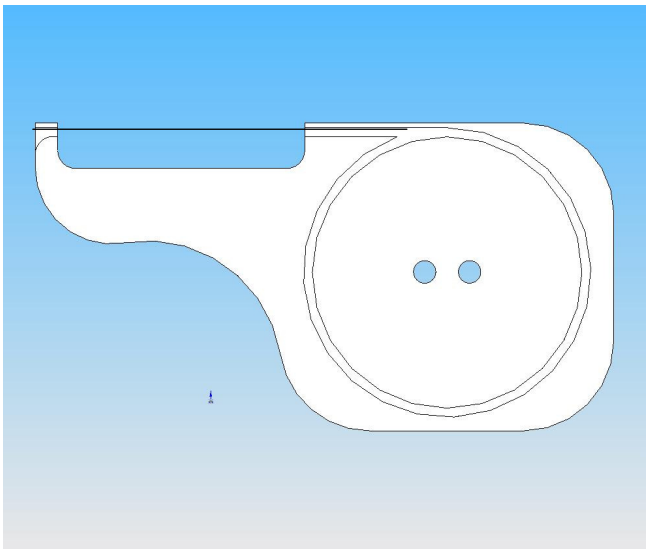

Fig 3.15 Plate holding fiber spool

Based on this design, the fiber is grasped about 2 to 2.5 inches away from the tip. This causes the fiber to sag towards the tip that is inserted into the package. To determine the exact nature of this problem, a testbed was setup as shown below.

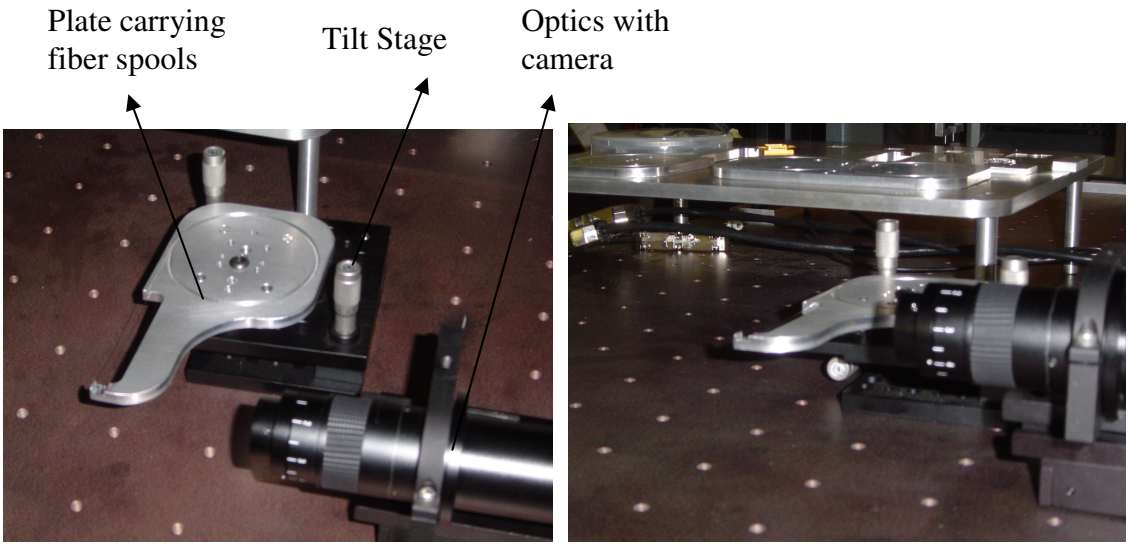

(a) (b)

Fig 3.16 Fiber tilt experiment test-bed; (a) top view, (b) side view

The tilt stage helps in pre-setting a tilt on the fiber to compensate for the sagging that occurs after lift. We start the experiment with no preset tilt much like how it is on the fiber insertion platform. The following two images show the fiber tip when the fiber is resting on the plate and after it is grasped/lifted for insertion.

The angle of this sag is measured to be within 1.04 degrees with the help of IMAQ ® vision tool. This error is way above the tolerance for any of the fiber related assembly operations (section 3.3). To minimize this angular error we use the tilt stage to incline the fiber by the same angle in its rest position so that after pick-up the fiber tip droops down to being horizontal. This experiment was repeated with different fiber samples

and using a preset tilt is found to reduce this pitch error to within 0.03 degrees which is within the tolerance specified for the package (refer table 3.2)

Table 3.2 Fiber tilt data

SL NO	Initial Angle -degrees (before using tilt stage)	Final Angle - degrees
1	1.0373	0.0212
2	1.0012	0.0299
3	1.0154	0.0271

G. Laser Fixture

The laser support fixtures are attached to the closed loop (three axes) robot. The Optical Imaging Accessory (OIA) is held in a fixture shown. The working distance of the laser is about 3 cms. This means that the fixture should compensate for the z difference from the bottom of the robot to about 2~4 cms from the focus point of the laser.

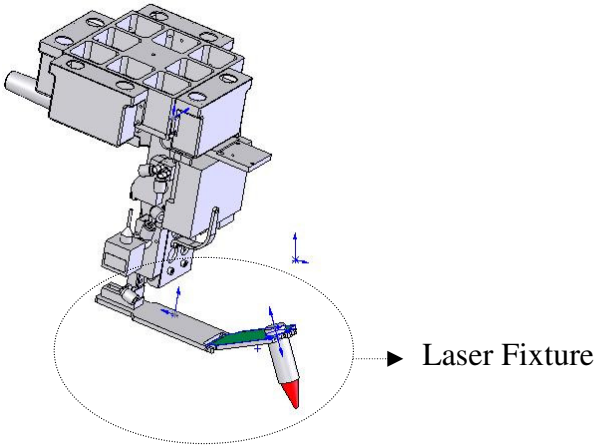

Fig3.17 Laser fixture

CHAPTER 4

SYSTEM ANALYSIS

4.1 End-Effector Performance

Background definitions of robot precision:

a. *Repeatability*: The range of actual positions that a robot goes to when given the same destination repeatedly.

b. *Accuracy*: The distance between the actual position in space to where the robot should have ideally gone.

c. *Resolution*: The smallest increment which can be made in a given motion.

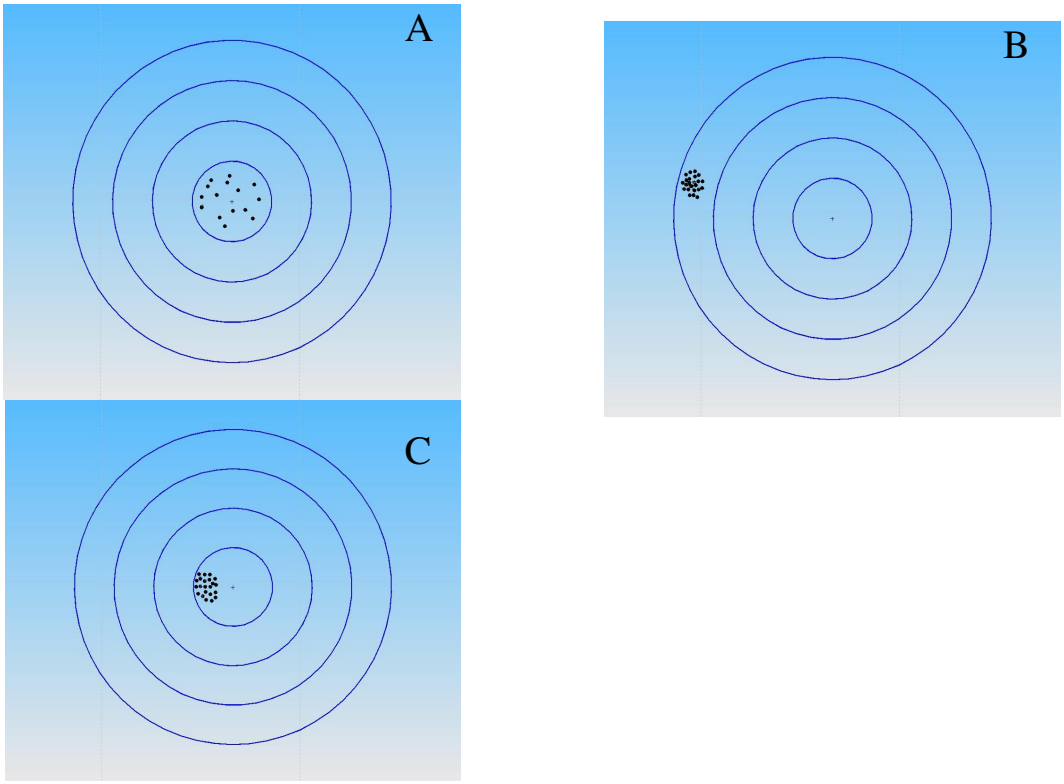

Figure 4.1 Bulls eye diagram;(a) good accuracy,(b)good repeatability,(c)ideal condition

Bulls Eye Diagram: The bulls eye diagram shows three different cases of robot positioning. In case A. the robot has poor repeatability but excellent accuracy. In case B the robot has good repeatability but is highly inaccurate. In case C, the robot has good accuracy and repeatability.

The tolerance budget for positioning of micro and mesoscale components is as shown in section 3.3. The coarse positioning robots (four axis and camera pucks) together with the fine positioning system should be able to work within this budget. In this section we determine the positioning accuracy of the coarse positioning system.

Accuracy/Repeatability Experiments on RobotWorld: We have performed experiments to determine the accuracy of any positioning system involving the usage of machine vision and encoder feedback. A component is picked up by the robot and brought underneath the camera with a pre-determined zoom level, and the camera is focussed on it as shown in figure 4.2.. On the corresponding CCD image seen, one feature convenient to be reliably used with machine vision is identified and saved as a template. An example of a template is shown. Shown in the picture is a trench into which an optic fiber is inserted. By repeated motions between two points, one of which is under the camera, we can match the template to what is seen each time and thus determine the accuracy.

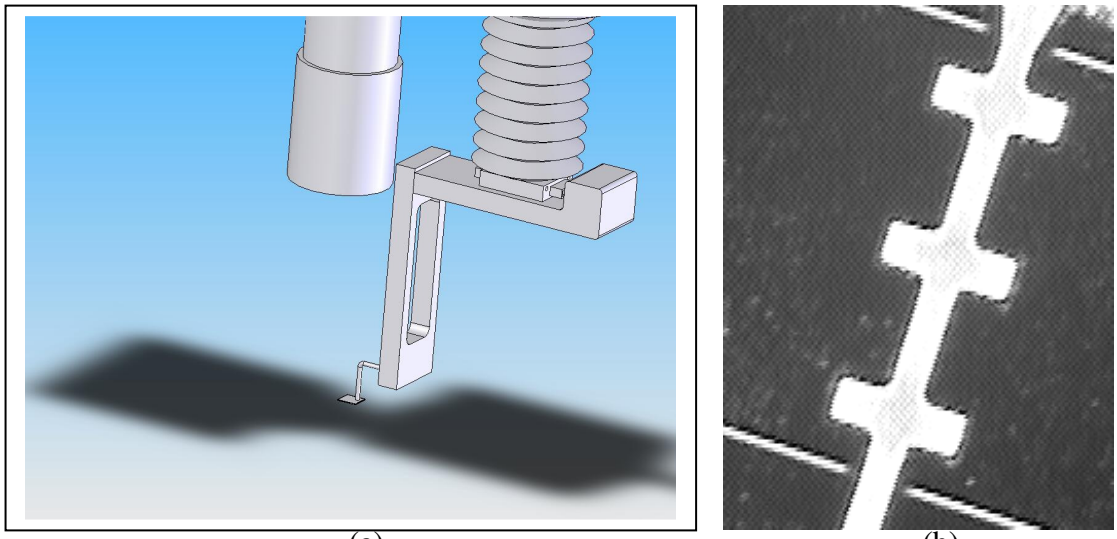

(a) (b)

Fig 4.2 Camera accuracy;(a) setup,(b)CCD image

Camera robot accuracy and repeatability test: The camera robot consists of the XY puck and the CCD with a motorized zoom microscope. In a setup such as this error can creep in two ways. One way is through the image capture and processing system (CCD + IMAQ® Machine vision software). This is determined by not moving anything (camera robot or component) and repeatedly capturing images of the same feature. The second source of error is the XY positioning system with the mechanical fixturing involved. This error is determined by repeatedly moving the camera robot between two points.

Type1: CCD accuracy (nothing moving). The above mentioned technique is followed and the error of the first kind is determined. The data obtained are tabulated. In the table shown Px and Py are the pixel readings for the CCD which

are transformed into RobotWorld coordinates X&Y using the transformation matrix described in the calibration section.

Table 4.1 CCD accuracy datapoints

Sl No:	Px	Py	X	Y
1	360	157.5	99.6063	99.2035
2	361.121	158.399	99.604	99.2011
3	361.179	158.455	99.6039	99.201
4	361.727	159.175	99.6021	99.1999
5	361.778	159.291	99.6018	99.1998
6	362.735	159.273	99.6018	99.1976
7	361.875	159.395	99.6015	99.1996
8	362.81	159.532	99.6012	99.1974
9	362.104	159.635	99.6009	99.1991
10	362.082	160.334	99.5992	99.1993

From the table shown above, the following error table is generated.

Table 4.2 CCD accuracy error

X(mm)	Y(mm)
-0.0023	-0.0024
-0.0024	-0.0025
-0.0042	-0.0036
-0.0045	-0.0037
-0.0045	-0.0059
-0.0048	-0.0039
-0.0051	-0.0061
-0.0054	-0.0044
-0.0071	-0.0042

From the data above the average errors in X and Y (X_m, Y_m) can be found.

X_m= 4.48 microns

Y_m= 4.08 microns

Standard deviation in X = 1.39

Standard deviation in Y= 1.21

The edumnd optics zoom camera has a resolution of 3.33 microns per pixel at 4X zoom and a FOV (field of view) of 2mm.

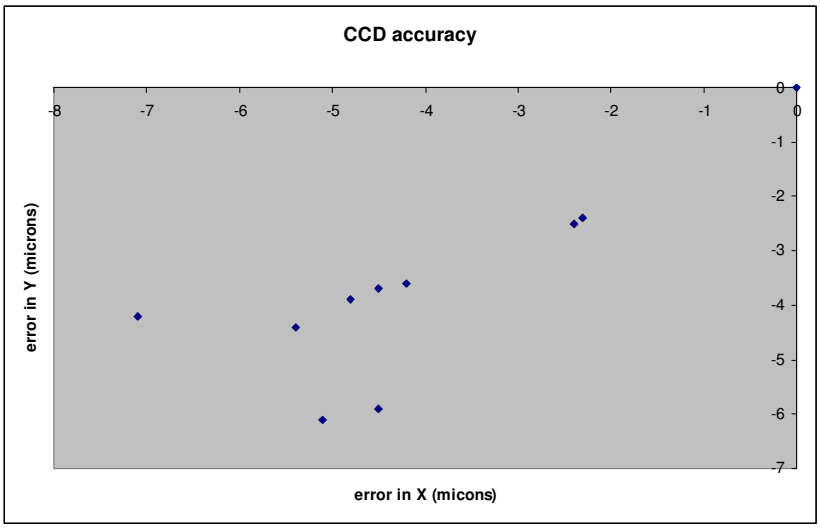

Fig 4.3 CCD accuracy datapoints

Type2: Camera Robot Repeatability: Xc and Yc are the camera robot coordinates in millimeters.

Table 4.3 Camera robot repeatability datapoints

Sl No:	Xc	Yc	Px	Py	X	Y
1	100	100	378.797	167.289	99.5818	99.1622
2	100	100	377.097	169.237	99.5769	99.1665
3	100	100	377.772	169.614	99.576	99.165
4	100	100	377.772	169.614	99.576	99.165
5	100	100	376.994	171.488	99.5713	99.1672
6	100	100	376.73	170.74	99.5731	99.1677
7	100	100	377.006	173.345	99.5666	99.1676
8	100	100	376.023	173.571	99.5661	99.1699
9	100	100	376.904	173.775	99.5656	99.1679
10	100	100	376.847	175.593	99.561	99.1684

From the experimental data points in the table shown above the following error table is generated.

Table 4.4 Camera robot repeatability error table

X(mm)	Y(mm)
-0.0049	0.0043
-0.0058	0.0028
-0.0058	0.0028
-0.0105	0.005
-0.0087	0.0055
-0.0152	0.0054
-0.0157	0.0077
-0.0162	0.0057
-0.0208	0.0062

From the data above the average errors in X and Y (X_m, Y_m) can be found.

X_m= 11.5 microns

Y_m= 5.04 microns

Standard deviation in X = 5.3

Standard deviation in Y= 1.48

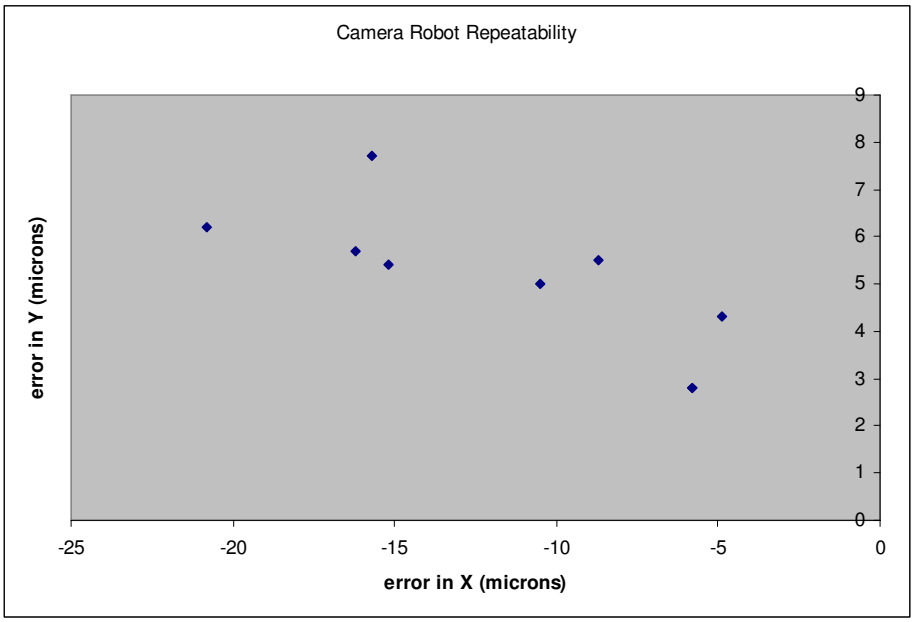

Fig 4.4 Camera robot repeatability datapoints

Robot Accuracy/Repeatability Test. Similar to the camera robot accuracy experiments, we can determine the error involved in moving the four axis robot with an end-effector. With focus on die-attach operation and considering the fact that most tools are used with this robot via quick change, we find the accuracy of this robot with the vacuum pick up tool that handles the die and the perform pick & place.

Type1: Point to Point Repeatability(without homing)*:* The robot is moved between two points one of which is monitored under the camera. While moving the robot between these two points, the robot is not homed or reset.

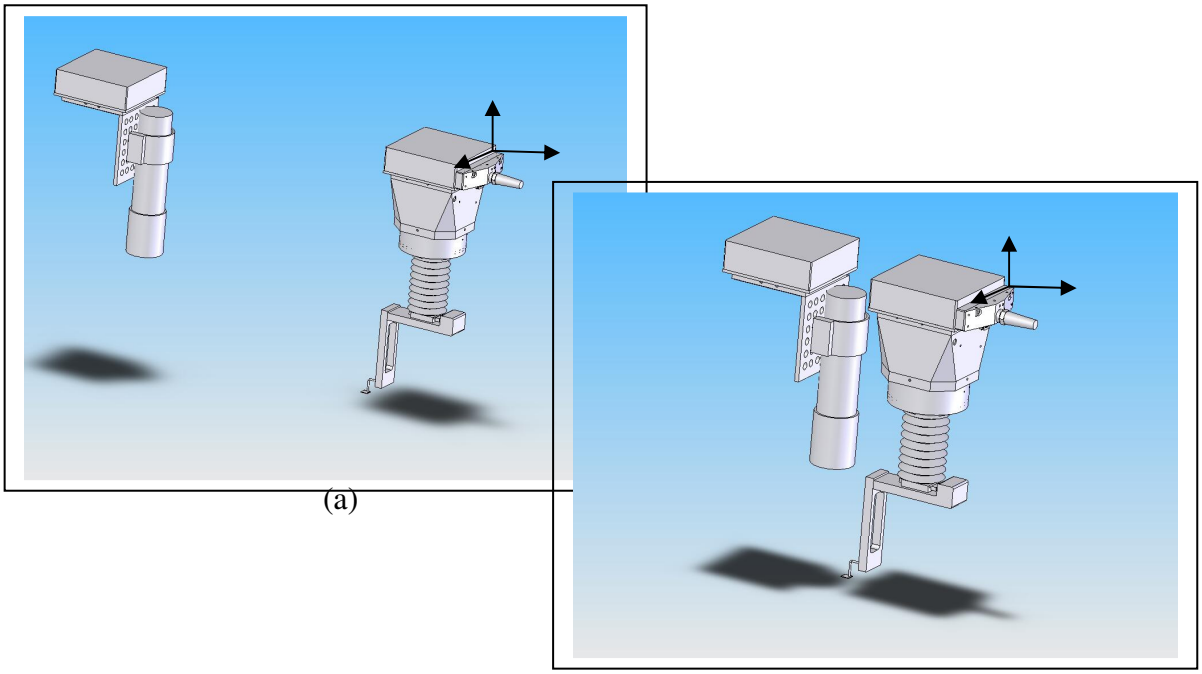

(a)

(b)

Fig 4.5 Robot Repeatability ;(a)Point1,(b)Point2

Point 1: X = 800mm

Y = 250.002mm

θ = 45.002 deg

Point 2: X = 679.251mm

Y = 167.656mm

θ = 10.824 deg

} under the camera

Table 4.5 Robot repeatability datapoints

Sl No:	Px	Py	X(mm)	Y(mm)
1	363.68	263.532	99.3412	99.2162
2	360.648	263.389	99.3415	99.2232
3	362.456	264.542	99.3386	99.2193
4	362.702	265.292	99.3368	99.2188
5	365.444	266.227	99.3344	99.2127
6	366.477	268.537	99.3287	99.2108
7	365.748	267.219	99.332	99.2122
8	365.696	267.511	99.3312	99.2124
9	367.419	267.364	99.3316	99.2084
10	366.478	268.521	99.3287	99.2108

Table 4.6 Robot repeatability error table:

X(mm)	Y(mm)
0.0003	0.007
-0.0026	0.0031
-0.0044	0.0026
-0.0068	-0.0035
-0.0125	-0.0054
-0.0092	-0.004
-0.01	-0.0038
-0.0096	-0.0078
-0.0125	-0.0054

From the data above the average errors in X and Y (X_m, Y_m) can be found.

X_m= 7.48 microns

Y_m= 1.91 microns

(Standard deviation in X = 4.29

Standard deviation in Y= 4.64)

The repeatability is 11.77 microns (sum of mean and standard deviation)

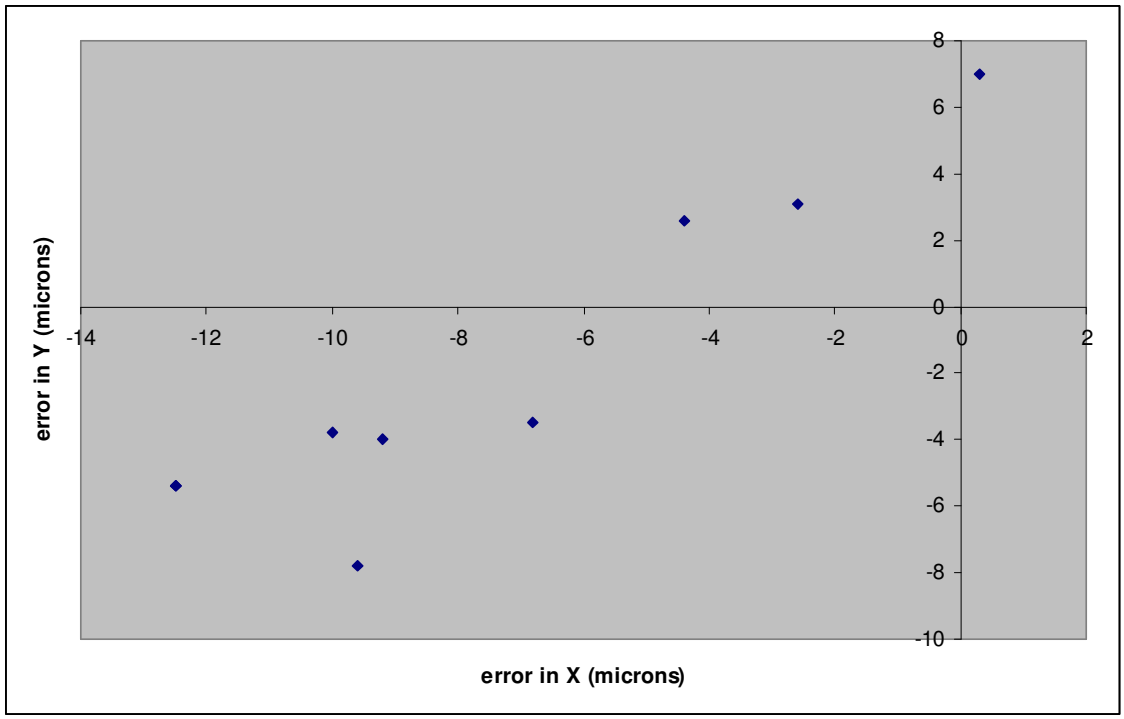

Fig 4.6 Robot repeatability datapoints

***Type2: Home to point via parts tray (Accuracy Test)*:** This experiment involves the following sequence of operations. a) Robot Initializes. b) Moves to tool rest and attaches to the vacuum pick-up tool via quick change. c) Moves to parts tray and picks up the MEMS die. d) Moves to a location and places the die under the camera. This sequence is repeated with the camera remaining in the exact same location. Each time machine vision is used to detect the location of a specific feature on the die. We

transform the pixel readings (Px and Py) into RobotWorld coordinates and measure the error.

Operating Conditions are Zoom=4X; Robot Speed =5mm/s and acc=0.1mm/s2

The coordinates of the four axis robot underneath the camera are

X = 1306.016 mm

Y = 717.176 mm

θ = 50.019 deg

The data points for this experiment are

Table 4.7 Robot accuracy datapoints

Sl No:	Px	Py	X (mm)	Y(mm)
1	282.5	303	99.2425	99.4108
2	282.523	303.828	99.2904	99.411
3	282.56	303.042	99.2424	99.4608
4	284.433	303.053	99.29	99.4064
5	284.461	303.001	99.3425	99.4063
6	282.523	303.828	99.2404	99.411

Table 4.8 Robot accuracy error table:

X(mm)	Y(mm)
0.0479	0.0002
-0.0001	0.05
0.0475	-0.0044
0.1	-0.0045
-0.0021	0.0002

From the data above the average errors in X and Y (X_m, Y_m) can be found.

X_m= 38.64 microns

Y_m= 8.3 microns

Standard deviation in X = 23.7

Standard deviation in Y= 20.9

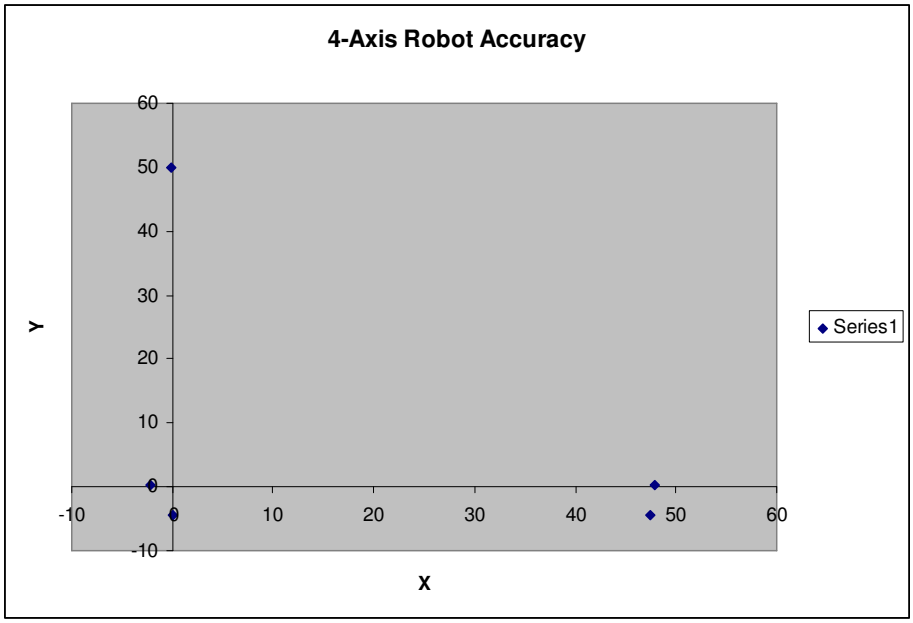

Figure 4.7 Four-axis robot accuracy

4.2 Calibration

The Multi-Scale assembly system consists of many different coordinate frames that are attached with different components that make up the system (robots, tools, fixtures and parts). Calibration is the procedure followed to represent all of these frames with respect to a single global coordinate frame. Once calibrated, any operation can be referenced with respect to this global coordinate frame. Robot calibration involves

identifying a functional relationship between the joint transducer readings and the actual workspace positions of the end effectors and using this to modify the robot control software [26]. From this standpoint calibration can be defined as a process by which robot accuracy is improved by modifying the robot positioning software rather than changing or altering the design of the robot or the control system. Calibration is a discrete event and is as such different from adaptive control where model identification is carried out continuously and controller parameters are adjusted in accordance with the identified changes.

In general calibration procedure consists of four steps. First step would be to choose a suitable functional relationship. This could be referred to as a modeling step. The second step would be to collect some data from the actual robot that relates the input of the model to the output. This step is termed as the measurement step. The third step is to use the data collected and mathematically calculate the unknown coefficients in the model. The final step would be the implementation of the model into the inverse kinematics for the robot.

The calibration method followed is the statistical calibration method which is an alternative to the model based approach of calibration. In this method the manipulator is commanded to many locations and the actual positions are recorded. From these two sets of values (commanded position and actual position) a mapping can be derived by doing a least squares fit on the data. We calibrate the robot to find out the relative location of the parts in the RobotWorld platen coordinate frame (see figure 4.4). We

have defined coordinate frames for all the different manipulators and for the part being manipulated.

The statistical calibration method comes with the following advantages;

1) There is no concern over stability of parametric representations.
2) This method can take into consideration error sources which are not due to geometric joint parameter errors, which leads to the possibility of this being a more accurate means of calibration.
3) Once calibrated the computation of positions is faster
4) This method facilitates modularity of the assembly system. Any changes in tool design can be easily accommodated in the calibration routine without focusing much on the exact nature of the change.

The following are the disadvantages that are associated;

1) We need to ensure that many locations are used to calibrate; so the process can be more tedious to begin with.
2) Little insight is given to the source of errors.

We find the transformation between the four axis manipulator coordinate system, the local coordinate frame on the MEMS die and the four axis camera robot coordinate frame. Finding this transformation reduces to a parameter identification problem for several unknown coefficients. A schematic diagram of the relative position of several local/global coordinate frames is shown in the figure here.

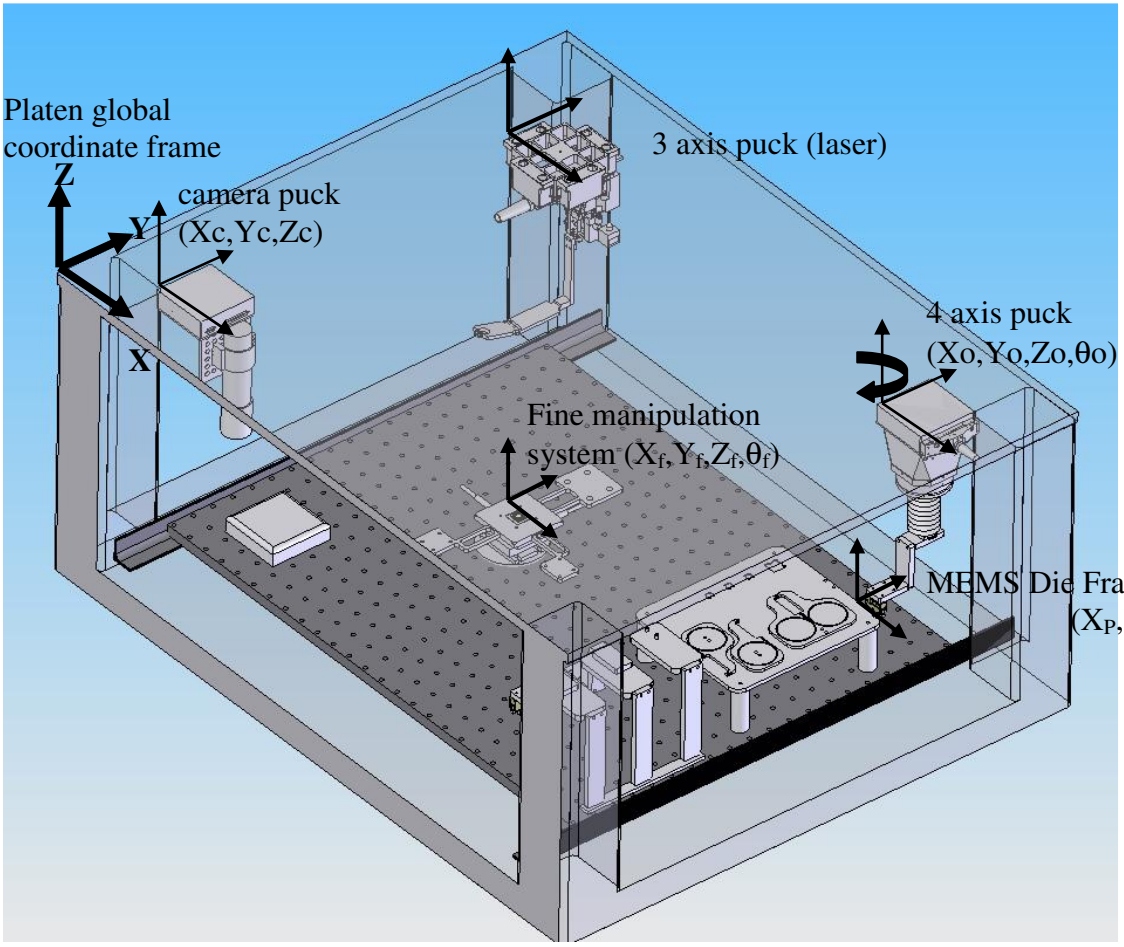

Fig 4.8 Assembly system coordinate frames

Calibration Routine for RobotWorld: As shown in the figure 4.5, consider the case when the camera is viewing a particular feature on the MEMS die on the four axis robot. For example, this feature could be the centric of a DRIE trench on the die. Let Xc, Yc, Zc be the joint coordinates of camera, Xo, Yo, Zo, θo be the joint coordinates for four axis robot, and Xp, Yp, Zp be the coordinates of the point in the platen coordinate frame.

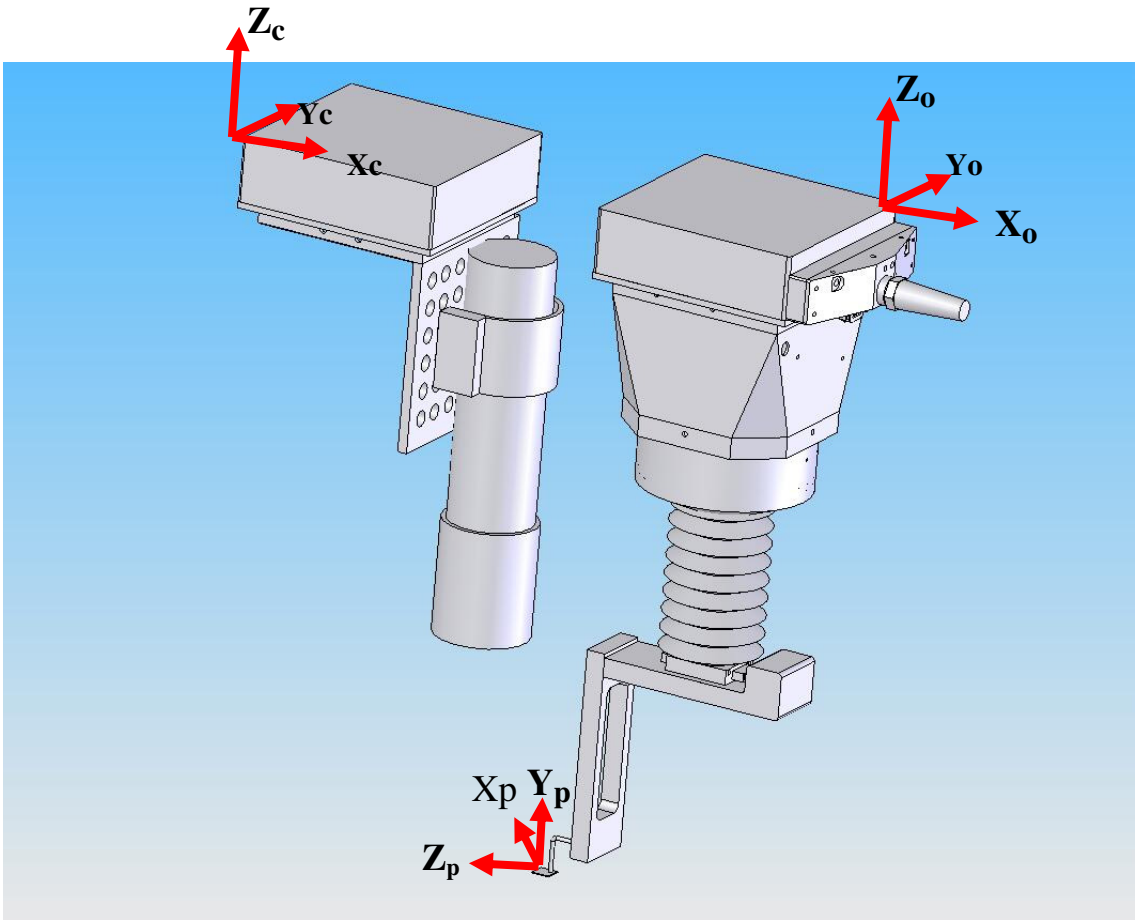

Fig 4.9 Camera/robot calibration

Camera Calibration

Experimental Procedure:

(a) Identify the die feature to be used (with which the die coordinate frame will be attached to)

(b) Move the camera to produce a grid of pixel coordinates (Pxi, Pyi)

(c) Record camera coordinates corresponding to pixel coordinates (Xci, Yci)

The platen (world) coordinates of the die (die feature) is given by

$$\begin{bmatrix} X_p \\ Y_p \end{bmatrix} = \begin{bmatrix} X_{ci} \\ Y_{ci} \end{bmatrix} + R_1 \begin{bmatrix} p_{xi} \\ p_{yi} \end{bmatrix} \qquad \ldots\ldots\ldots\ldots (1)$$

For repeated readings, the (Xp, Yp) coordinates remain the same. Hence

$$0 = \begin{bmatrix} \Delta Xci \\ \Delta Yci \end{bmatrix} + R1 \begin{bmatrix} \Delta p_{xi} \\ \Delta p_{yi} \end{bmatrix} \qquad \text{……..(2)}$$

The above equation can be re-written as

$$\begin{bmatrix} \Delta p_{xi} & \Delta p_{yi} & 0 & 0 \\ 0 & 0 & \Delta pi & \Delta p_{yi} \end{bmatrix} \begin{bmatrix} r11 \\ r12 \\ r21 \\ r22 \end{bmatrix} = -\begin{bmatrix} \Delta X_{ci} \\ \Delta Y_{ci} \end{bmatrix} \qquad \text{……....(3)}$$

For ‘n+1’ trials; the above equation can be extended to

$$\begin{bmatrix} \Delta p_{x1} & \Delta p_{y1} & 0 & 0 \\ 0 & 0 & \Delta p_{x1} & \Delta p_{y1} \\ \Delta p_{x2} & \Delta p_{y2} & 0 & 0 \\ 0 & 0 & \Delta p_{x2} & \Delta p_{y2} \\ \vdots & \vdots & \vdots & \vdots \\ \Delta p_{xN} & \Delta p_{yN} & 0 & 0 \\ 0 & 0 & \Delta p_{xN} & \Delta p_{yN} \end{bmatrix} \begin{bmatrix} r11 \\ r12 \\ r21 \\ r22 \end{bmatrix} = -\begin{bmatrix} \Delta X_{c1} \\ \Delta Y_{c1} \\ \Delta X_{c2} \\ \Delta Y_{c2} \\ \vdots \\ \Delta X_{cN} \\ \Delta Y_{cN} \end{bmatrix} \qquad \text{…….……(4)}$$

Re-writing the above equation,

$$[w] \begin{bmatrix} r_{11} \\ r_{12} \\ r_{21} \\ r_{22} \end{bmatrix} = [v] \qquad \text{……..(5)}$$

Unknowns are r11, r12, r21, r22.

We can solve this as a least squares fit on the data known using the pseudo-inverse method. Thus we can map the die in the world coordinate frame. The identification of the R matrix thus completes the calibration of the camera robot.

5 DOF manipulator calibration:

$$\begin{bmatrix} Xp \\ Yp \\ 1 \end{bmatrix} = \begin{bmatrix} Xo \\ Yo \\ 1 \end{bmatrix} + \begin{bmatrix} k1 \\ k2 \\ 0 \end{bmatrix} + {}^{0}\mathrm{T}_{N}(\theta) \begin{bmatrix} P_{xinit} \\ P_{yinit} \\ 1 \end{bmatrix} \qquad \ldots\ldots\ldots\ldots (6)$$

'${}^{O}T_{N}$' is the transformation matrix that relates the CCD pixel coordinate frame to the robot coordinate frame. It accounts for rotation and scaling. 'k1' and 'k2' are the translation factors.

Comparing this equation with equation(1),

$$\begin{bmatrix} Xp \\ Yp \\ 1 \end{bmatrix} = \begin{bmatrix} Xo \\ Yo \\ 1 \end{bmatrix} + \begin{bmatrix} k1 \\ k2 \\ 0 \end{bmatrix} + \begin{bmatrix} R & T \\ 0 & 1 \end{bmatrix} \begin{bmatrix} P_{xinit} \\ P_{yinit} \\ 1 \end{bmatrix} \quad = \begin{bmatrix} Xc \\ Yc \\ 1 \end{bmatrix} + R1 \begin{bmatrix} P_{xinit} \\ P_{yinit} \\ 1 \end{bmatrix} \qquad \ldots\ldots\ldots\ldots (7)$$

P_{xinint} and P_{yinit} are the first set of pixel coordinates as seen by the CCD. The transformation matrix '${}^{O}T_{N}$' is represented by rotation matrix R and translation matrix T. This rotation matrix is further represented in terms of R(θi) which is the subsequest rotations involved.

$$\begin{bmatrix} Xc \\ Yc \\ 1 \end{bmatrix} + \begin{bmatrix} R1 & 0 \\ 0 & 1 \end{bmatrix} \begin{bmatrix} P_{xinit} \\ P_{yinit} \\ 1 \end{bmatrix} = \begin{bmatrix} Xo \\ Yo \\ 1 \end{bmatrix} + \begin{bmatrix} k1 \\ k2 \\ 0 \end{bmatrix} + \begin{bmatrix} R(\theta_1) & 0 \\ 0 & 1 \end{bmatrix} \begin{bmatrix} R1 & T \\ 0 & 1 \end{bmatrix} \begin{bmatrix} P_{xinit} \\ P_{yinit} \\ 1 \end{bmatrix}$$

..... (8)

$$\begin{bmatrix} Xc \\ Yc \end{bmatrix} + R1 \begin{bmatrix} P_{xi} \\ P_{yi} \end{bmatrix} = \begin{bmatrix} X_{oi} \\ Y_{oi} \end{bmatrix} + \begin{bmatrix} k1 \\ k2 \end{bmatrix} + R(\theta_i).R1 \begin{bmatrix} P_{xinit} \\ P_{yinit} \end{bmatrix} + R(\theta_i) \begin{bmatrix} t_1 \\ t_2 \end{bmatrix}$$

..... (9)

$$\begin{bmatrix} I_2 & R(\theta_i) \end{bmatrix} \begin{bmatrix} k1 \\ k2 \\ t1 \\ t2 \end{bmatrix} = \begin{bmatrix} Xc \\ Yc \end{bmatrix} + R1 \begin{bmatrix} Pxi \\ Pyi \end{bmatrix} - \begin{bmatrix} Xoi \\ Yoi \end{bmatrix} - R(\theta_i) R1 \begin{bmatrix} Pxinit \\ Pyinit \end{bmatrix} \text{..... (10)}$$

$$\begin{bmatrix} I_1 & R(\theta_1) \\ I_2 & R(\theta_2) \\ ..... & \\ ..... & \\ ..... & \\ I_n & R(\theta n) \end{bmatrix} \begin{bmatrix} k1 \\ k2 \\ t1 \\ t2 \end{bmatrix} = \begin{bmatrix} v_1(Xo1, Yo1, \theta 1) \\ v_2(Xo2, Yo2, \theta 2) \\ .... \\ .... \\ .... \\ v_n(Xon, Yon, \theta n) \end{bmatrix} \quad \text{..... (11)}$$

implies that the unknown matrix is given by

$$\begin{bmatrix} k1 \\ k2 \\ t1 \\ t2 \end{bmatrix} \qquad \ldots\ldots\ldots\ldots (12)$$

using the pseudo inverse function (least squares method) we can compute this matrix.

A Matlab® code is written and used to solve for the above unknowns using least square fit. This completes the calibration procedure required.

Calibration Implementation: The calibration procedure described above is implemented with the following details.

Step1: Camera Calibration

The operating conditions are as follows; Zoom=4X, Robot speed=10mm/s and robot acceleration= 0.1mm/s2.

Table 4.9 Camera and pixel coordinates for grid

SL NO	Xc-mm	Yc-mm	Px	Py
1	100	100	421	221.5
2	99.25	100	428.116	374.431
3	99.75	100	423.271	273.455
4	99.75	100.25	372.772	272.852
5	99.25	100.25	377.798	373.624
6	100	100.25	370.693	223.823
7	100	100.5	314.765	222.369
8	99.75	100.5	315.88	271.935
9	99.25	100.5	321.164	372.673

For the grid shown above, the camera calibration results in the following transformation matrix;

$$R1 = \begin{pmatrix} 0.0001 & 0.0050 \\ 0.0047 & -0.0002 \end{pmatrix}$$

Step 2a: Robot Calibration (8 point calibration)

Operating Conditions

Robot Speed	5 mm/s
Acceleration	0.1mm/s2

All dimensions in mm

Table 4.10 Eight point calibration datapoints

SL NO	variable	Xo	Yo	θ –deg	Px	Py	Xc	Yc
1		599.021	305.327	77.498	421.634	222.729	100	100
2	x	599.493	305.327	77.498	425.685	325.611	100	100
3	y	599.493	304.751	77.498	308.367	323.351	100	100
4	θ	599.493	304.751	77.14	396.221	161.525	100	100
5	x,θ	599.153	304.751	77.752	245.757	368.669	100	100
6	x,y	598.499	306.001	77.746	497.827	235.384	100	100
7	y,θ	598.499	305.002	77.453	366.04	105.449	100	100
8	x.y,θ	599.743	304	77.002	282.732	155.685	100	100

The transformation matrix that results from the calibration procedure followed is

$$\begin{pmatrix} k1 \\ k2 \\ t1 \\ t2 \end{pmatrix} = \begin{pmatrix} -421.5726 \\ -77.2245 \\ -77.4068 \\ -128.0874 \end{pmatrix}$$

Calibration Verification:

Table 4.11 Calibration Datapoints

SL NO	Xo	Yo	θ	Px	Py	Xc	Yc
1	600	304	77.008	283.805	208.689	100	100
2	600	305	77.349	402.152	361.555	100	100
3	600	304.5	77.352	236.235	211.35	100.75	100.25
4	600.5	304.25	77.358	395.355	212.395	101.25	99.25

For the data points shown above, the following errors are obtained from the calibration equations;

Table 4.12 Calibration Error

ErrorX	ErrorY
5.4083	13.8928
4.2309	-6.6493
20.4007	2.831
-5.2499	6.7048

The eight point calibration technique yields a LSE residue of 20.4 microns.

Since we require that the residue be within the sum of repeatability of four axis puck + repeatability of camera puck, which is 11.77 + 5.87=17.64 microns, the increase the grid size used for robot calibration such that the variance is reduced below the threshold of 17.64 microns. So we next try the 27 point calibration where in we form a 3X3X3 grid of variants (X, Y, and Theta).

Step2b. 27 Point Calibration: For similar operating conditions, the following datapoints are collected.

Table 4.13 Twenty seven point calibration datapoints

SL NO	Xo	Yo	θ	Px	Py	Xc(mm)	Yc(mm)
1	679	168	11.002	272.5	135.5	104.9	102.569
2	679	168	10.9	387.236	141.386	104.9	102.569
3	679	168	10.8	488.792	147.48	104.9	102.569
4	679	167.751	11.002	175.517	138.722	104.9	102.569
5	679	167.751	10.894	283.302	146.328	104.9	102.569
6	679	167.751	10.811	389.359	153.283	104.9	102.569
7	679	167.65	11.002	137.715	146.337	104.9	102.569
8	679	167.65	10.9	245.211	151.448	104.9	102.569
9	679	167.65	10.83	322.381	157.433	104.9	102.569
10	679.249	167.999	11.008	297.602	244.431	104.9	102.569
11	679.249	167.999	10.9	402.766	250.562	104.9	102.569
12	679.249	167.999	10.83	472.389	247.22	104.9	102.569
13	679.249	167.751	11.002	190.481	239.658	104.9	102.569
14	679.249	167.751	10.9	301.101	247.606	104.9	102.569
15	679.249	167.751	10.843	367.341	252.269	104.9	102.569
16	679.249	167.653	11.008	150.936	243.553	104.9	102.569
17	679.249	167.653	10.9	261.697	250.412	104.9	102.569
18	679.249	167.653	10.83	332.53	255.21	104.9	102.569
19	679.499	168	11.002	301.592	350.484	104.9	102.569
20	679.499	168	10.9	417.548	358.339	104.9	102.569
21	679.499	168	10.83	490.274	363.324	104.9	102.569
22	679.499	167.751	11.002	200.452	355.724	104.9	102.569
23	679.499	167.751	10.894	316.618	363.39	104.9	102.569
24	679.499	167.751	10.83	389.438	368.304	104.9	102.569
25	679.499	167.656	11.008	174.625	358.393	104.9	102.569
26	679.499	167.656	10.9	279.353	365.61	104.9	102.569
27	679.499	167.656	10.83	350.634	370.258	104.9	102.569

This procedure yields a LSE residue of about 11 microns which is well below the threshold variance figure of 17.64 microns set by the camera and the four axis manipulator. With reference to the tolerance budget explained in section 3.3, this calibration technique can be employed for the die to package assembly, Top Chip to Die assembly and the Indium Preform to package assembly.

The decision to employ calibration, fixturing or visual servoing can be based on the following design rules

a. Fixtures can be used to locate objects in the assembly only when the manipulator accuracy is smaller than the required part or feature tolerance.
b. Calibration can be used to locate objects in the workspace only if the repeatability of the manipulator is smaller than the tolerance required.
c. Visual Servoing on the relative position between parts and tools can be used only if the resolution of the manipulator is smaller than the tolerance required

4.3 PID gain tuning/Tool oscillations

The PID gain values of the controller are tuned to minimize the effect of oscillations. The PID values are changes and the tool performance is observed under the zoom microscope. This way the values are optimized. Gain tuning is particularly important when the tools include high inertia and offsets. Also, gain tuning is performed for all the tools with the robot that handle them.

4.4 Inverse Kinematics

Forward Kinematics (or direct kinematics) is the process of computing the position and orientation of the tool relative to the global coordinate frame given the joint angles of the manipulator. A greater challenge is to work a suitable set of values for the robot joints to achieve a required tool position. This procedure is called Inverse Kinematics.

So far we have worked towards determining the accuracy and repeatability of the positioning systems and towards expressing the various coordinate frames with respect to the platen coordinate frame. We have also determined that the four axis robot with the vacuum pick-up tool can be calibrated within the tolerance limit required for die-attach. Next, we need to implement calibration such that using the zoom microscope and the four axis robot (at the appropriate joint angles) accomplish die attach.

We use constrained least square solution to numerically calculate the pose of the robot necessary to align the MEMS die to the package as follows:

1. We first image the location of the fiber feedthroughs on a Kovar carrier package. We use the NI IMAQ library to compute the position of a point situated in the center of three of the fiber feedthrough (one on each side of the package). These locations are computed using the COARSE-2 calibration data to be at global coordinates (Xpj, Ypj, Zpj), where $1 \leq j \leq 3$.
2. We then present a MEMS die to the camera puck and we image the three corresponding points in the center of the DRIE trenches. In pixel coordinates, these points are at (Pxij, Pyij) initial coordinates.
3. We then solve the constrained LSE problem to find the joint coordinates of the COARSE-2 manipulator that minimizes the error vector represented by the length difference between points on the die and points on the package expressed in global coordinates. We want to find Xo, Yo, and θo that minimize:

$$\min_{X_o, Y_o, \theta_o} \sum_{j=1}^{3} \left(\begin{bmatrix} X_{pj} \\ Y_{pj} \end{bmatrix} - \begin{bmatrix} X_o \\ Y_o \end{bmatrix} - \begin{bmatrix} k_1 \\ k_2 \end{bmatrix} - R(\theta_o)\left(M_1 \begin{bmatrix} p_{xij} \\ p_{yij} \end{bmatrix} + \begin{bmatrix} t_1 \\ t_2 \end{bmatrix} \right) \right)^2 \quad \text{..... (12)}$$

$$R(\theta_o) = \begin{bmatrix} \cos(\theta_o) & -\sin(\theta_o) \\ \sin(\theta_o) & \cos(\theta_o) \end{bmatrix},$$

by assigning $z_1 = X_o, z_2 = Y_o, z_3 = \cos(\theta_o), z_4 = \sin(\theta_o)$, we can reduce the inverse kinematics problem to the following constrained LSE:

$$\min_{\substack{z_1, z_2, z_3, z_4 \\ z_3^2 + z_4^2 = 1}} \sum_{j=1}^{3} \left(\begin{bmatrix} z_1 \\ z_2 \end{bmatrix} + \begin{bmatrix} c_{1j} & c_{2j} \\ c_{2j} & -c_{1j} \end{bmatrix} \begin{bmatrix} z_3 \\ z_4 \end{bmatrix} - \begin{bmatrix} v_{1j} \\ v_{2j} \end{bmatrix} \right)^2$$

where C1j, C2j, V1j, and V2j are coefficients depending on calibrated kinematics and feature locations in pixel coordinates. This constrained LSE has an exact solution that can be found using Lagrange multipliers and the eigenvalue of a residual matrix. However, during our die-package attach experiments we used a numerical solution instead, based on the LSQNONLIN function of MATLAB.

CHAPTER 5

CONCLUSIONS AND FUTURE WORK

A robotic assembly cell with multi-scale capability has been developed to perform a packaging assignment. The tolerance budget of the package has been studied. Various mechanical tools and fixtures have been designed, built and tested , followed by repeatability tests, which have been conducted to determine the exact positioning accuracy of the robots and vision system. Calibration has been implemented to work within the required tolerances. The four-axis robot accuracy is repeatable within 8 microns with the vacuum pickup tool and the vision system accuracy is 11.5 microns. Statistical calibration results in variance being limited to 11 microns. Based on the accuracy, repeatability and calibration experiments, we conclude that for die attach, calibration is to be implemented and fixturing alone is not sufficient. For fiber insertion, we visual servoing is the suggested technique to be followed. An inverse kinematics solution has been developed for the four-axis robot with die handling tool to accomplish die attach within acceptable accuracy limits.

This work can be continued to implement visual servoing for applications that demand higher precision such as the fiber insertion into the trench within a tolerance of 4 microns. Also, statistical calibration needs to be further studied with regards to optimizing the number of datapoints required to calibrate any given system. Also, reformulation of the assembly sequencer using a discrete event controller (DEC)

framework can be implemented. The mechanical design of the tools can be improved to better suit the application and also to suit modularity need.

REFERENCES

1. “Micro and Meso Scale Robotic Assembly”, Dan O. Popa and Harry E. Stephanou, Center for Automation Technologies, Rensselaer Polytechnic Institute, Troy, New York, USA

2. Feddema, J.T. Simon, R.W. , “Visual servoing and CAD-driven microassembly,” in Robotics & Automation Magazine, Vol. 5, Issue 4, pp. 18-24, Dec. 1998.

3. Y. Zhou, B.J. Nelson, B. Vikramaditya, “Fusing Force and Vision Feedback for Micromanipulation,” in Proc. of IEEE Conf. On Robotics and Automation (ICRA ’98), Leuven, Belgium, 1998

4. Y. Ge, J.A. Gaines, B.J. Nelson, “Open-structure reconfigurable experimental work-station for fast and reliable microassembly,” in SPIE Proc. Microrobotics and Microassembly II, Boston, MA, Nov. 2000, pp.21-32.

5. S.J. Ralis, B. Vikramaditya, B. J. Nelson, “Micropositioning of a Weakly Calibrated Microassembly System Using Coarse-to-Fine Visual Servoing Strategies,” in IEEE Transactions on Electronics Packaging Manufacturing, Vol 23, No.2, April 2000.

6. R.Eberhardt, T. Scheller, et., al., “Automated assembly of microoptical components,” SPIE Proc. Microrobotics and Mycrosystem Fabrication, vol 3202, pp. 117-127, Pittsburgh, USA, 1997

7. Bleuler, H., Clavel, R., Breguet, J. M., Langen, H., & Pernette, E., "Issues in precision motion control and microhandling," In IEEE proceedings of ICRA, San Francisco, CA, (pp. 959–964).

8. H. Bleuler, J.-M. Breguet, "Microfactory and Microrobotics Activities in Europe", in International Workshop on Micro-Factory (IWMF), Tsukuba, Japan, 1998.

9. T.Hirano, K. Furata, "Micromachine technology trends in microfactory," in International Workshop on Micro-Factory (IWMF), Minneapolis, Sept 2002

10. R. Hollis, J. Gowdy, "Miniature Factories for Precision Assembly," in Proc. Int'l Workshop on Micro-Factories, Tsukuba, Japan, December 7-8, 1998.

11. D.O. Popa, B.H. Kang, J. Sin, "Reconfigurable Microassembly System for Photonics Applications," in Proc. IEEE Conf. on Robotics and Automation, Washington, D.C., 2002

12. D.O. Popa, et., al., "Dynamic Modeling and Open-Loop Control Of Thermal Bimorph MEMS Actuators," in Proc. IEEE Conf. on Robotics and Automation, Taipei, Taiwan, 2003.

13. A.A. Rizzi, J. Gowdy, R.L. Hollis, "Agile assembly architecture: an agent based approach to modular precision assembly systems," in Proc. of 1997 IEEE International Conference on Robotics and Automation, Volume: 2 , 20-25 April 1997, Pages:1511 – 1516

14. M.B. Cohn, et.,al., "Microassembly Technologies for MEMS," SPIE Micromachining and Microfabrication, Santa Clara, CA (September 1998

15. S. Fatikow , J. Seyfried1 , St. Fahlbusch1 , A. Buerkle1 and F. Schmoeckel1 , “A Flexible Microrobot-Based Microassembly Station,” in Journal of Intelligent and Robotic Systems, Vol 27, No. 1-2, January 2000
16. K. Goldberg, K.F. Bohringer, R. Fearing, “MicroAssembly,” in Handbook of Industrial Robotics, 2nd Edition, edited by S. Nof. John Wiley and Sons, 1999. pp 1045-1066
17. Y. Bellouard, “Microrobotics, Microdevices Based on Shape-Memory Alloys,” in Encyclopedia of Smart Materials, Wiley, pp. 620-644, 2002
18. M. Mikawa, “Visual Servoing for Micro Mass Axis Alignment Device,” in Proc. of IEEE/RSJ International Conference on Intelligent Robots and Systems (IROS), 1996, pp.1091-1096.
19. N. Isam N. Tahhan, Yan Zhuang, K.F. Bohringer, K.S.J. Pister, K. Goldberg, “MEMS Fixtures for Handling and Assembly of Microparts,” SPIE's 1999 Symposium on Micromachining and Microfabrication, Santa Clara, California. September, 1999.
20. O. T. Strand, M. E. Lowry, “Automated Fiber Pigtailing Technology,” Electronic Components and Technology Conference, 1994, pp.1000-1003.
21. C. R. Witham, “Fiber-Optic Pigtail Assembly and Attachment Alignment Shift Using a Low-Cost Robotic Platform,” Electronic Components and Technology Conf., 2000, pp21-25.
22. S. Jang, “Automation Manufacturing Systems Technology for Opto-electronic Device Packaging,” Electronic Components and Technology Conf., 2000, pp.10-14.

23. D.O. Popa, M. Deeds, et. al., " Automated Assembly and Hermetic Packaging of MOEMS for Applications Requiring Extended Self-Lives," in Proc. of ASME IMECE, November 5-11, 2005

24. C. Mavroids, et., al., " A Systematic Error Analysis of Robotic Manipulators: Application to a High Performance Medical Robot", Proceedings of the 1997 International Conference in Robotics and Automation, Albuquerque, NM, April, 1997.

25. Slocum A., "Precision Machine Design"., Englewood Cliffs 1992

26. Brad Nelson et.,al., "Visual Servoing for Robotic Assembly", in Visual Servoing-Real-Time Control of Robot Manipulators Based on Visual Sensory Feedback, ed. K.Hashimoto, World Scientific Publishing Co. Pte. Ltd., River Edge, NJ, pp. 139-164, 1993.

BIOGRAPHICAL INFORMATION

Rakesh Murthy was awarded a Bachelor's degree in Mechanical Engineering from Rashtreeya Vidhyalaya College of Engineering, Bangalore, India in 2002 and a Master's degree in Mechanical Engineering from the University of Texas at Arlington in 2005. He is currently pursuing PhD in Electrical Engineering at the University of Texas at Arlington. He can be contacted at the following email address: rakesh@arri.uta.edu